EFFECT OF PHASE TRANSFORMATION ON THE FRACTURE BEHAVIOR OF SHAPE MEMORY ALLOYS

A Thesis

by

ANTONINO FRANCESCO PARRINELLO

Submitted to the Office of Graduate Studies of
Texas A&M University
in partial fulfillment of the requirements for the degree of

MASTER OF SCIENCE

Chair of Committee,	Dimitris C. Lagoudas
Committee Members,	John Whitcomb
	Junuthula N. Reddy
Head of Department,	Rodney Bowersox

August 2013

Major Subject: Aerospace Engineering

ABSTRACT

Over the last few decades, Shape Memory Alloys (SMAs) have been increasingly explored in order to take advantage of their unique properties (*i.e.,* pseudoelasticity and shape memory effect), in various actuation, sensing and absorption applications. In order to achieve an effective design of SMA-based devices a thorough investigation of their behavior in the presence of cracks is needed. In particular, it is important to understand the effect of phase transformation on their fracture response.

The aim of the present work is to study the effect of stress-induced as well as thermo-mechanically-induced phase transformation on several characteristics of the fracture response of SMAs. The SMA thermomechanical response is modeled through an existing constitutive phenomenological model, developed within the framework of continuum thermodynamics, which has been implemented in a finite element framework.

The effect of stress-induced phase transformation on the mechanical fields in the vicinity of a *stationary* crack and on the toughness enhancement associated with crack *advance* in an SMA subjected to in-plane mode I loading conditions is examined. The small scale transformation assumption is employed in the analysis according to which the size of the region occupied by the transformed material forming close to the crack tip is small compared to any characteristic length of the problem (*i.e* the size of the transformation zone is thirty times smaller than the size of the cracked ligament). Given this assumption, displacement boundary conditions, corresponding to the Irwin's solution for linear elastic fracture mechanics, are applied on a circular region in the austenitic phase that encloses the stress-induced phase transformation zone. The quasi-static stable crack growth is studied by assuming that the crack

propagates at a certain critical level of the crack-tip energy release rate. The Virtual Crack Closure Technique (VCCT) is employed to calculate the energy release rate. Fracture toughness enhancement associated with transformation dissipation is observed and its sensitivity on the variation of key characteristic non-dimensional parameters related to the constitutive response is investigated. Moreover, the effect of the dissipation due plastic deformation on the fracture resistance is analyzed by using a Cohesive Zone Model (CZM).

The effect of thermo-mechanically-induced transformation on the driving force for crack growth is analyzed in an infinite center-cracked SMA plate subjected to thermal actuation under isobaric mode I loading. The crack-tip energy release rate is identified as the driving force for crack growth and is measured over the entire thermal cycle by means of the VCCT. A substantial increase of the crack-tip energy release rate – an order of magnitude for some material systems – is observed during actuation as a result of phase transformation, *i.e.*, martensitic transformation occurring during actuation causes anti-shielding that might cause the energy release rate to reach the critical value for crack growth. A strong dependence of the crack-tip energy release rate on the variation of the thermomechanical parameters characterizing the material response is examined. Therefore, it is implied that the actual shape of the strain-temperature curve is important for the quantitative determination of the change of the crack-tip energy release rate during actuation.

ACKNOWLEDGEMENTS

I used to remind myself: *If you want to achieve something special during your lifetime, if you really want your name to be remembered, you have to have talent for what you decide to pursue, the will to work hard and great people supporting you in your efforts.*

I want to take this opportunity to thank all the people who have supported me during my journey towards the achievement a dream which now becomes real: the Master of Science Degree in Aerospace Engineering from Texas A&M University.

I first want to thank my parents, Bartolo e Rita, most of all. They represented a constant source of moral support throughout my entire life. I am grateful to them teaching me the value of education and hard work as essential steps to make my dreams real. I thank them for having suffered with me all the *battles* I went through and for always reminding me they will always be there for me regardless at the circumstances.

I also want to thank my lovely sister Rossana. Since I was a kid, she has supported me in every single moment, even when my way of acting did not deserve it. For all her love and care I want to say thanks.

Leaving my country of origin, Italy, to pursue a higher education at Texas A&M, was concurrently a tough choice to make and an exciting challenge to pursue. I embarked in this adventure aware of all the difficulties I would have face without losing spirit and motivation. My wish to join the Aerospace Engineering Department at Texas A&M was mainly driven by the desire to work under the supervision of Dr. Dimitris Lagoudas. I will never forget the first day in which I met him: his charisma and devotion to research confirmed that I could have never been more fortunate.

Therefore, I want to express my gratitude to him for giving me the chance to enhance my skills by working as a research assistant in his research group. I have no doubt in stating that he is one of the main authors of my success. He was always a driving force in my pursuit for becoming not only a better scientist but also a better person. I would like also to thank him for believing in my abilities for becoming a successful researcher.

I could never thank enough Dr. Theocharis Bexevanis for all the support he gave me. As my supervisor, Theo constantly followed my work with passion and patience. He taught me the beauty of mechanics and how all the related disciplines apply to solve real engineering problems. I want to share the merit for this achievement with him since he inspired most of the research topics which we worked on together. Over the last two years, Theo has been an invaluable guide, a mentor and most importantly a true friend. I have always appreciated his honesty even when our discussions went out of the lines, I have always felt there was no lying in him and that he is someone who I can always trust. Surely, he is one of the reasons why I could make it this far. He indelibly contributed to my personal and scientific growth for which I will never let the memory of him depart.

During my time at Texas A&M, I have had the pleasure of meeting and working with several great people. I would like to extend my gratitude towards all the members of the Shape Memory Alloys Research Team. In particular, I would like to thank my dear friends Frank, Majid and Austin who have shared all my suffering and complaints in Wisenbaker. I would like also to acknowledge the valuable support of Dr. Darren Hartl. Through a constant interaction with him, I was able to improve my engineering creativeness and strengthen passion for science. I would like also to thank Dr. Junuthula Reddy for all the support provided over the course of my studies and Dr. John Whitcomb for having kindly joined my committee.

I would like to acknowledge the support received by the International Institute of Materials for Energy Conversion (IIMEC) led by Dr. Dimitris Lagoudas. Through this support, I had the chance to carry on in my research and present my work at multiple international events. The international nature of this institution gave me the opportunity to interact with a variety of researchers who enhanced my scientific perspectives.

I also would like to thank my best friends Michele and Rukshan who, even though not physically present at my side, shared with me all the victories and defeats which I encountered through out the course of my experiences. I hope this is a starting point to build a bright future together.

Finally, I thank Stefania Occhipinti. She definitely deserves the best share of all my achievements. I do not think I could have accomplished 6 years of aerospace engineering studies without having her with me. I could not even imagine what my life would have been without her positive attitude and care. She climbed the route towards the "top of the mountain" with me by making plenty of sacrifices even when my purposes and ambitions were not clear in her eyes. I jealously preserve her in my heart and consider all the memories as one of the most important treasures in my life.

TABLE OF CONTENTS

LIST OF FIGURES

FIGURE Page

LIST OF TABLES

TABLE Page

1. INTRODUCTION AND LITERATURE REVIEW*

Progress in technology and science is increasingly demanding materials for complex applications. Engineers have always pursued the goal of improving functional efficiency of structural systems by looking at innovative design and materials. During the last few decades, researchers have probed the use of active materials to improve the structural performance, reduce the complexity of the compound and also provide other functionalities such as sensing and actuation. Among the variety of active materials which have been investigated, Shape Memory Alloys (SMAs) have been on the forefront of research since their discovery.

SMAs are a unique class of metallic based alloys capable of converting thermal energy to mechanical work and vice versa. The unique behavior of SMAs is attributed to their ability to recover large amount of strains. The key physical mechanism that drives this shape recovery is a reversible diffusionless solid to solid microstructural phase transformation from austenite to martensite and vice-versa under applied load or temperature variations. Over the past twenty years, SMAs have been increasingly used in a wide range of actuation, energy absorption and vibration damping applications in the aerospace, civil and medical industries [80, 59, 35]. Therefore, the interest in analyzing their response in the presence of cracks has grown. In particular a thorough understanding of the effect of phase transformation on their fracture behavior is needed for an effective design of SMA components. Few studies have focused on investigating the effect of stress-induced phase transformation on the fracture properties of SMAs by either experimental or theoretical approaches while thermo-

*Part of this chapter is reprinted with permission from "On the fracture toughness enhancement due to stress-induced phase transformation in shape memory alloys" by Baxevanis, T., Parrinello, A.F., Lagoudas, D.C., 2013, International Journal of Plasticity. doi: http://dx.doi.org/10.1016/j.ijplas.2013.04.007

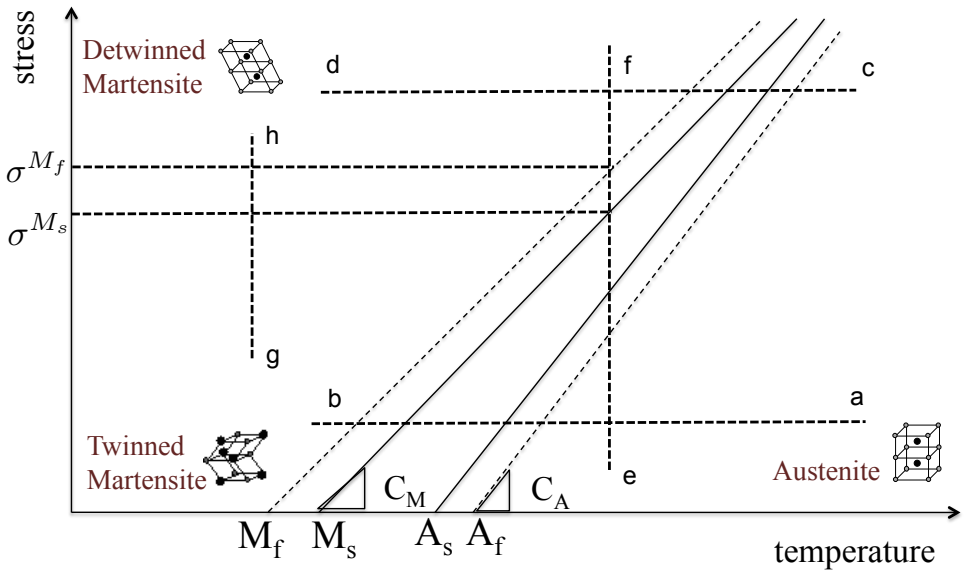

Figure 1.1: Stress–temperature phase diagram

mechanically-induced phase transformation has not been addressed yet. The former has been motivated by the need to understand the fracture behavior of SMAs when their pseudoelastic response is desirable in application such as vibration dampers and biomedical stents. The latter concerns the desire to effectively use SMAs in thermal actuators applications.

1.1 Phase Transformation in Shape Memory Alloys

It is possible, to summarize SMAs unique behavior into two main categories: Pseudoelasticity and Shape Memory Effect. The former is related to the recovery of large strains upon mechanical loading and unloading at temperatures where the austenitic parent phase exists stably at zero load. The latter refers to the ability of the material to thermally recover deformations initially generated by either (i) applying a mechanical loading/unloading cycle at low temperature, or (ii) cooling/heating the material under stress from austenite to martensite [64, 47]. Shape

memory alloys are characterized by a diffusionless phase transformation of their lattice crystal structures from an high symmetry cubic *parent* phase (austenite), to a low symmetry *product* phase (martensite). The parent phase, which generally exist at high temperatures, has a cubic structure while the product phase can have a a tetragonal, orthorhombic or monoclinic crystal structure. Upon certain loading conditions, the material can reverse transform from the martensitic to the austenitic phase. Phase transformation can be described in a schematic fashion in the two dimensional temperature-stress space by means of a phase diagram as presented in Figure 1.1. The transformation surfaces are plotted as lines with slopes C_M, C_M and identify the borders of thermodynamic state at which both the phases coexist stably in the material. When a decrease in the temperature is imposed, an initially austenitic material starts transforming into martensite at a temperature M_s and becomes full martensite when the temperature M_f is reached. It has to be noted that at zero or low stress levels the transformation results in *twinned* martensite ($a \rightarrow b$) which is characterized by the presence of different variants of martensite with different orientations in a self accommodate fashion such that no change in the shape of the material is observed. However, if the change in the temperature is applied at higher stress levels, transformation leads to the formation of *detwinned* martensite ($c \rightarrow d$) in which a preferred variant, according to the direction of the stress, is predominant and a significant shape change occurs because of the higher lattice distortion. Along the same lines, reverse transformation to austenite begins when the material is heated up to the temperature A_s and completes when temperatures above A_f are reached ($d \rightarrow c$). Martensitic transformation can also be induced by directly applying stress to an initially austenitic material throughout isothermal loading path. Hence the material points undergo stress-induced martensitic transformation when the critical stress value σ^{M_s} is reached whereas the full martensitic state is achieved at a stress

level equal or above σ^{M_f} $(e \rightarrow f)$. Reverse phase transformation from martensite to austenite occurs when upon unloading the material reaches certain stress levels such that the martensite transformation surfaces are crossed $(f \rightarrow e)$. Moreover, the reorientation of martensitic variants can be achieved under applied stress such that self-accomodated martesite transform into detwinned martensite $(g \rightarrow h)$ in which all the variants are consumed in favor of one single variant oriented according to the direction of the applied stress. The initial austenitic state is finally achievable if the detwinned martensite is subjected to an increase in the temperature.

1.2 Literature Review on Fracture Mechanics of SMAs

As the use of SMAs has risen substantially, the interest in understanding their fracture behavior has grown. Gall et al. [30] studied the fracture behavior of precipitated single crystal and polycrystalline NiTi specimens. It was found that the main failure mechanisms consist of a combination of nucleation, growth and coalescence of voids and brittle cleavage along preferential crystalline directions. It was pointed out that one mechanism takes over the other one depending on the size of the precipitates. In particular, small coherent precipitates lead to a more remarked cleavage type of failure while larger precipitates result in a more predominant ductile failure. It was also reported that a pronounced ductility can be associated with the generation of plastic deformation induced by intergranular constraints. However, a more significant brittle behavior emerges because of the tendency of each grain to behave as an individual homogenous single crystal which fractures mostly by cleavage. Several experimental and numerical works have had the aim to gain a thorough understanding of the effect of phase transformation on their fracture properties. In nominally isothermal conditions, stress-induced phase transformation is expected near the crack tip where the stress field is in theory unbounded. Crack-tip stress-induced marten-

sitic transformation was reported by Robertson et al. [74] and Gollerthan et al. [33] in superelastic polycrystalline NiTi compact tension experiments using in situ X-ray microdiffraction measurements under plane stress and plane strain conditions, respectively. The shape and size of crack-tip transformation zone was assessed by digital image correlation in the work of Daly et al. [22] and Taillebot et al. [87]. Martensitic transformation was also observed close to the notch tip in single crystal NiTi notched tensile specimens using optical techniques in situ by Creuziger et al. [21]. Nucleation of stress-induced phase transformation at the crack tip was demonstrated analytically in Bulbich [17] to be possible only during slow subcritical crack growth. The crack-tip stress-induced phase transformation is primarily responsible for the phenomenon of stable crack growth in SMAs under monotonically increasing load or displacement conditions, as shown in the experimental investigation of the fracture toughening behavior of an NiTi tube by Robertson and Ritchie [73]. As the crack advances in SMAs, material elements near the crack tip are transformed resulting in dissipated energy that must be supplied by the external loading in order to maintain crack growth. This enhancement of fracture toughness occurs over the crack growth range of a few times the maximum height of the transformation zone at initiation of crack propagation.

Several analytical works used a linear elasticity based approach to estimate the stress redistribution due to stress-induced martensitic transformation around an initially austenitic material subjected to isothermal loading conditions and containing a stationary crack. Most of these works focused on mode I loading of *static* cracked in superelastic SMAs ([11, 100, 53, 56, 57, 52, 51]) adopt Irwin's correction of LEFM. Baxevanis and Lagoudas [9] proposed a model along the lines of the Dugdale model [26] developed for conventional elastic-plastic materials. A critical applied load level was found, below which austenite is not fully transformed in the vicinity of the crack

tip. For applied load levels above the critical value, the size of the plastic zone was found to be between 0% and 80% of the size anticipated in conventional elastic-plastic materials. The two extremes correspond to a load level equal to the critical value (0%) and to large-scale transformation conditions (80%) in which almost the whole material has been transformed from austenite to martensite. Closed form expressions of the J-integral depending on the applied load level were obtained and parametric studies on the size of the plastic and transformed regions formed in front of the crack tip were conducted.

Numerical simulation was also used to study the phase transformation fields near static cracks by the finite element method [96, 94, 95, 8]. In their calculations, Wang et al. [96] neglected plasticity and showed that the extent of the transformation zone is load path-dependent due to the hysteretic stress-strain behavior of SMAs and that the formation of martensite results in a redistribution process where the stresses near the crack tip relax. In the work of Wang [94, 95], an elastic-plastic material model based on the von Mises yield criterion was calibrated by an experimental monotonic tensile stress-strain relation to account for both transformation and plasticity. The calculations showed that martensite transformation increases the required load to produce plastic deformation and decreases the maximum normal stress near the crack tip. Baxevanis et al. [8] used a constitutive material behavior that accounts for both phase transformation and plastic deformation to study the mechanical fields near the crack tip and the dependence of the size and shape of the transformation zone on the variation of characteristic thermomechanical parameters and temperature. The size of the plastic zone was found to be an order of magnitude less than the size anticipated in conventional elastic-plastic materials. The mechanical fields close to the crack tip were shown to recover the typical behavior of a power-law hardening material as in the asymptotic solution (HRR field) found by Hutchinson [39] and

Rice and Rosengren [72]. The J-integral was evaluated on various integration paths around the crack tip and found to be path-dependent. However, from an engineering point of view, the assumption of a fracture toughness criterion for SMAs based on the path-independence of the J-integral, a common practice in conventional elastic-plastic materials, could be justified in the sense that the difference between the crack-tip and far-field J-values in SMAs was found to be smaller than the corresponding difference in elastic-plastic materials.

There are only few theoretical and numerical investigations on the toughening effect of stress-induced phase transformation associated with crack advance in SMAs. Yi and Gao [102] and Yi et al. [103], based on the micromechanical constitutive equations of Sun and Hwang [86, 85], studied the fracture toughness of martensitic SMAs in mode I and mixed mode conditions. The transformation volume strain was assumed negligible compared to the transformation shear strain, and was thus ignored. Their analyses followed closely that of McMeeking and Evans [58] and Budniansky et al. [16] using Linear Elastic Fracture Mechanics (LEFM) theory together with the Eshelby equivalent inclusion method to obtain resistance curves. Transformation toughening was found to be associated with crack advance, due to the irreversible transformed region left behind by a quasi-statically advancing crack tip. Stam and van der Giessen [82] investigated the effect of stress-induced phase transformation on the crack growth resistance of SMAs for mode I loading by implementing the constitutive model proposed by Sun et al. [84] in a finite element framework using a nodal release approach. The fracture toughness enhancement due to martensitic transformation was evaluated by measuring the ratio of the far-field stress intensity factor to the crack-tip stress intensity factor. The near-tip intensity reduction was calculated by integrating over the transformation zone an analytical expression for the stress intensity reduction/enhancement caused by in-plane stress-free transfor-

mation strains in an infinitesimal area at any point within the transformation zone [48]. Freed et al. [29] used the phenomenological constitutive equations of Panoskaltsis et al. [63] and cohesive elements to model crack growth. It was found that the choice of the cohesive strength has a great influence on the toughening behavior of the SMAs. Baxevanis et. al [10] studied the steady state crack growth in pseudoelastic SMAs for a different range of operational temperature including those in which reverse phase transformation might occur due to unloading in the wake of the crack. Reverse phase transformation distinguishes the toughening response of SMAs from that of other dissipative materials displaying similar response, such as conventional elastic-plastic materials and ferroelastics. Reverse phase transformation being a dissipative process itself increases the toughness enhancement. However, for increasing temperatures, although the material's tendency to reverse transform increases, so does the critical stress level required for martensitic transformation which has the opposite effect on the toughening response of SMAs. The net outcome is lower fracture toughness enhancement for increasing nominal temperatures

It has to be noticed that, most of the works concerning the fracture behavior of SMAs have focused on mechanical loading conditions at nominally constant temperatures. To the knowledge of the author, up to now there have not been works addressing the effect of thermo-mechanically-induced phase transformation on the fracture behavior of SMAs. However, the topic is of crucial importance since the effective use of SMAs in actuators applications requires an understanding of their fracture and actuation-fatigue-crack growth properties under thermal loading. SMA actuators take advantage of thermo-mechanically-induced phase transformation to provide a significant amount of actuation with an extremely small envelope volume. SMA actuators are therefore used as an alternative to electromagnetic actuators when a small volume and/or large force and stroke are required and thermodynamic

efficiency is not essential [36, 81, 61].

1.3 Objective of the Present Work

In this work, the effect of stress-induced and thermo-mechanically-induced phase transformation several characteristics of the fracture behavior of SMAs is analyzed through a computational approach. The rest of the thesis is organized as follows:

- In chapter 2 a review of the constitutive modeling approaches proposed to study SMA response is provided. The SMA constitutive model proposed by Lagoudas and coworkers [44] is considered. The model is developed within the framework of continuum thermodynamics and makes use of internal state variables to take into account the evolution of phase transformation. The response of the material is taken to be characteristic of polycrystalline SMAs where the generation and recovery of all martensitic variants is described in a volume average sense. Moreover, a discussion related to its implementation in the ABAQUS [1] finite element framework is presented.

- In chapter 3 finite element analyses are carried out to study the mechanical fields around a stationary crack in a material initially in the austenitic phase subjected to isothermal plane strain, mode I loading conditions. A region of stress-induced martensite is expected to form around the crack tip where the stress are theoretically unbounded. The boundary layer approach is used in the calculations by restricting the transformation to be much smaller than all the length scales involved in the problem. In particular, displacement boundary conditions, corresponding to the asymptotic Irwin solution for the linear elastic fracture mechanics (LFEM), are applied on a circular region that encloses the stress-induced phase transformation zone which forms around the crack tip. Moreover, the quasi static stable crack growth is studied adopting the crit-

ical crack tip energy release rate as a fracture criterion which is measured through the VCCT. The fracture toughness enhancement associated with the dissipation due to phase transformation is measured in terms of the ratio of the far-field energy release rate to the crack-tip energy release. The sensitivity of fracture toughness enhancement on several characteristic non-dimensional parameters identified in the constitutive model is investigated. Furthermore, the effect of the dissipation due plastic deformations on the fracture resistance is analyzed by using a Cohesive Zone Model.

- Chapter 4 concerns the study of the effect of thermo-mechanically-induced global phase transformation (actuation) on the crack driving force of an SMA material. The sensitivity of the driving force for crack growth in SMAs is analyzed by considering the infinite center-cracked plate prototype. Phase transformation is induced by applying isobaric thermal variations. In particular, a material in an initial austenitic state at temperature T_h above the austenitic finish temperature (A_f) is first mechanically loaded and then subjected to a global thermal cycle. The temperature is decreased below the martensitic finish temperature (M_f) and then increased again in order to reach the initial value, T_h. The effect of phase transformation on the crack tip energy release rate, which is representative of the driving force for crack growth, is measured over the entire thermal cycle through the VCCT. As an outcome a substantial increase of the energy release rate, an order of magnitude for some material systems, is observed during cooling due to martensitic transformation. The effect of several characteristic non-dimensional parameters on the crack tip energy release rate is investigated. A detailed representation of the mechanical fields near the static crack is also provided.

- Chapter 5 contains some conclusions and underlines some of the key findings of the present work. Moreover, some of the future challenges are proposed.

2. CONSTITUTIVE MODEL FOR POLYCRYSTALLINE SHAPE MEMORY ALLOYS

Over the last few decades, several researchers have proposed different approaches to model the thermomechanical response of polycrystalline SMAs. These approaches can be divided into two main classes: the micromechanics based models and the phenomenological ones.

2.1 Overview of Constitutive Modeling Approaches

As far as micromechanical based models are concerned, it is aimed to model the overall SMA response by considering the different microstructural characteristics of the crystals existing within the material. For instance, given enough information concerning the microstructure, a constitutive theory developed to study the behavior of a single crystal can be employed to analyze the polycrystalline response. However, describing all the features of the microstructure is a difficult task to accomplish; also, the computational costs required to model the overall response of the material raise as the complexities involved in its characterization increase. Moreover, when a polycrystalline material systems is considered, intergranular incompatibilities and different crystallographical orientations have to be taken into account. In order to overcome these difficulties, homogenization techniques can be employed to achieve the response of the material at the structural level. Along these lines Patoor et al. [65], Falk [27], Lagoudas and Bhattacharya [23] and Gao and Brinson [31], have proposed constitutive models which use self-consistent averaging approaches to calculate the effective thermomechanical response of the polycrystalline material.

Phenomenological constitutive models are developed within the framework of continuum thermodynamics and employ internal variables to describe how the state

of the material evolves during phase transformation. In order to obtain the set of equations required to predict the material response, a free energy (*i.e* Helmothz free energy or Gibbs free energy) which depends on the quantities chosen to characterize the state of the material (*i.e.* stress, strain, temperature and internal variables) is usually assumed. By using the laws thermodynamics in conjunction with classical arguments such as the Coleman-Noll procedure [20], it is possible to get a set of relations between all the variables (*i.e.,* the constitutive equations for the SMA response). Furthermore, evolution equations are postulated to describe the rate of change of the microstructure. Experimental investigations, such as mechanical and isobaric actuation tests, are needed to calibrate the whole set of model parameters needed to fully reproduce the thermomechanical response. Phenomenological models have been extensively developed and refined to address several aspects of the behavior of polycrystalline SMAs. The asymmetry in the tensile and compressive response has been studied by Raniecki and Lexcellent [4] and Qidwai and Lagoudas [67] by investigating the effect of different forms for the transformation function. The detwinning of self-accomodated martensite under applied mechanical loading has been addressed and included in a three dimensional phenomenological model by Leclercq and Lexcellent [50] and Popov and Lagoudas [66]. The SMA thermomechanical response under non-proportional loading conditions has been studied by Arghavani et al. [3] and Bouvet et. al [12]. A detailed survey concerning most of the works related to the phenomenological modeling of the behavior of SMAs can be found in the work of Lagoudas et al [45]. Nevertheless, some of the constitutive models reported in the literature can be associated to the same thermodynamics framework as long as they employ the same set of state variables to describe the evolution of the SMA state. However, they can be distinguished from each other because of the different choice in the hardening function adopted to describe the phase transition. For instance, the

constitutive model originally proposed by Boyd and Lagoudas [13, 15, 14] employed a linear hardening function which can be replaced by an exponential form or cosine form to incorporate, within the same framework, the models proposed by Tanaka et al [88, 42] and Liang and Rogers [55], respectively. Finally, it has to be remarked that, the use of phenomenological approaches has increasingly resulted in successful modeling efforts due to the relatively straightforward numerical implementation within a finite element framework.

2.2 Constitutive Model

The proposed model relies on the unified model for polycrystalline SMAs proposed by [13]. It is developed within the framework of continuum thermodynamics and adopts the classical rate-independent small-strain flow theory (*i.e.,* J_2 flow type theory) for the evolution equations of the transformation strains.

Assuming an isotropic elastic response for the SMA, the increments of the total strain tensor components, $d\varepsilon_{ij}$, are given as

$$d\varepsilon_{ij} = S_{ijkl} d\sigma_{kl} + dS_{ijkl}\sigma_{kl} + d\varepsilon^{t}_{ij} + d\varepsilon^{the}_{ij}, \tag{2.2.1}$$

where σ_{ij}, ε^{t}_{ij} are the Cartensian components of the stress tensor and of the transformation strain tensor, respectively, ε^{the}_{ij} are the components of the stress-free thermal strain due to thermal expansion. S_{ijkl} are the components of the 'current' compliance tensor. The standard Einstein notation is used with summation over repeated indices assumed. The 'current' compliance tensor varies with the martensite volume fraction ξ as $S_{ijkl} = (1-\xi)S^{A}_{ijkl} + \xi S^{M}_{ijkl}$, where S^{A}_{ijkl} and S^{M}_{ijkl} are the components of the compliance tensor of pure austenite and martensite phases, respectively. The assumption of elastic isotropy for both the austenitic and martensitic phases reads as $S^{\alpha}_{ijkl} = \frac{1+\nu_\alpha}{2E_\alpha}(\delta_{il}\delta_{jk} + \delta_{ik}\delta_{jl}) - \frac{\nu_\alpha}{E_\alpha}\delta_{ij}\delta_{kl}$, where the index α stands for A in the case

of austenite and for M in the case of martensite. E_α, ν_α denote the Young's modulus and Poisson's ratio of the two phases, respectively, and δ_{ij} is Kronecker's delta.

An evolution equation of the transformation strain is defined so that it is related to the evolution of martensite volume fraction, ξ, a

$$d\varepsilon_{ij}^t = \Lambda_{ij} d\xi, \quad \Lambda_{ij} = \begin{cases} \Lambda_{ij}^{fwd}, \ d\xi > 0, \\ \\ \Lambda_{ij}^{rev}, \ d\xi < 0, \end{cases} \tag{2.2.2}$$

where, Λ_{ij}, the components of the direction tensor, are defined as

$$\Lambda_{ij}^{fwd} = \frac{3}{2} \frac{H^{cur}}{\bar{\sigma}} s_{ij}, \quad \Lambda_{ij}^{rev} = \frac{\varepsilon_{ij}^{t-r}}{\xi^{t-r}}. \tag{2.2.3}$$

Here, H^{cur} is the uniaxial transformation strain magnitude for complete transformation, $\bar{\sigma} = \sqrt{\frac{3}{2} s_{ij} s_{ij}}$ is the Mises equivalent stress and $s_{ij} = \sigma_{ij} - \sigma_{kk}\delta_{ij}/3$ are the stress deviator components. Also, ε_{ij}^{t-r} and ξ^{t-r} are the transformation strain and martensitic volume fraction at the point of reversal of the transformation. During forward transformation, the transformation strain is oriented by the direction of the deviatoric stress, which motivates the selected J_2 form of the direction tensor. During reverse phase transformation, it is assumed that the direction and magnitude of the transformation strain recovery is governed by the average orientation of the martensite at transformation reversal (the cessation of forward transformation, be it partial or full). This definition allows to return to a zero transformation strain for every state with a null martensite volume fraction. H^{cur} is a function of the stress state since most SMA materials do not exhibit a constant maximum attainable transformation strain at all stress levels. A saturated value of maximum attainable transformation strain is reached at a high stress level, which is dependent

on the SMA material as well as the processing conditions for a polycrystalline material, resulting in different crystallographic and morphological textures, for example. Following this observation, the maximum transformation strain H^{cur} is represented by the following decaying exponential function

$$H^{cur}(\bar{\sigma}) = H_{sat}\left(1 - e^{-k\bar{\sigma}}\right), \tag{2.2.4}$$

where the parameter H_{sat} describes the ultimate transformation strain given a uniaxial loading (*i.e.*, the maximum recoverable strain generated such that increases in stress magnitude do not increase the transformation strain). The parameter k controls the rate at which H^{cur} exponentially evolves from 0 to H_{sat}.

During transformation, the stress tensor components should remain on the transformation surface

$$\Phi = 0, \;\; \Phi = \begin{cases} \Phi^{fwd} = \pi^{fwd} - Y_0, \; d\xi > 0, \\ \\ \Phi^{rev} = -\pi^{rev} - Y_0, \; d\xi < 0, \end{cases} \tag{2.2.5}$$

with π^{fwd}, π^{rev} being the thermodynamic driving forces for forward and reverse transformation, respectively, and Y_0 is the critical value of the thermodynamic force to both initiate and sustain forward and reverse phase transformation. The thermodynamic driving force for forward transformation is written as

$$\pi^{fwd} = \sigma_{ij}\Lambda_{ij}^{fwd} + \frac{1}{2}\Delta S_{ijkl}\sigma_{ij}\sigma_{kl} + \sigma_{ij}\Delta\alpha(T - T_0) + \rho\Delta s_0 T - \rho\Delta u_0 - f^{fwd}, \tag{2.2.6}$$

where

$$f^{fwd}(\xi) = \alpha_1\xi + \alpha_3, \tag{2.2.7}$$

and for reverse transformation

$$\pi^{rev} = \sigma_{ij}\Lambda_{ij}^{rev} + \frac{1}{2}\Delta S_{ijkl}\sigma_{ij}\sigma_{kl} + \sigma_{ij}\Delta\alpha(T - T_0) + \rho\Delta s_0 T - \rho\Delta u_0 - f^{rev}, \quad (2.2.8)$$

where

$$f^{rev}(\xi) = \alpha_2\xi - \alpha_3. \quad (2.2.9)$$

f^{fwd} and f^{rev} are functions describing the transformation hardening behavior during forward and reverse phase transformation, respectively. s_0 and u_0 are the specific entropy and internal energy at a reference state, respectively. ρ is the density and it is assumed the same for both the phases, Δ denotes the difference in property between the martensitic and the austenitic states, and α_i $(i = 1, 2, 3)$ are coefficients that assume real number values.

Given these constitutive relations the following model parameters must be calibrated: (i) the elastic parameters of martensite and austenite, (ii) parameters contained in the functional form of the maximum transformation strain $H^{cur}(\bar{\sigma})$, and (iii) six model parameters ($\rho\Delta s_0$, $\rho\Delta u_0$, α_1, α_2, α_3, Y_0) that are characteristic of the martensitic transformation. The common material properties that are used to calibrate the model are E_A, E_M, ν_A, ν_M, H, M_s, M_f, A_s, A_f, C_M, and C_A. M_s, M_f, A_s and A_f are the martensitic-start, martensitic-finish, austenitic-start and austenitic-finish temperatures at zero load, respectively, and C_M and C_A are the forward and reverse transformation slopes in the stress–temperature phase diagram, respectively (Figure 1.1). The elastic constants can be calculated directly from isothermal stress–strain curves where loads are applied at temperatures outside the transformation regions. The parameters for $H^{cur}(\bar{\sigma})$ can be calibrated directly from isobaric material testing, where the value of k in particular is chosen to best fit the experimental

trend. The remaining six parameters are calibrated by considering the conditions under which forward transformation begins and ends in the stress–temperature or stress–strain space [46].

2.3 Numerical Implementation

In the following, a brief overview of the methodology used to implement the constitutive model within a finite element framework is given. The constitutive model has been implemented in a customized user material subroutine (UMAT) in order to be used in conjunction with the ABAQUS finite element suite to solve a variety of boundary value problems. The UMAT receives as input the current strain and increment of strain, as well as temperature and increment of temperature from the solver and provides the updated state of stress and the current tangent moduli which have to be computed at every increment due to the highly nonlinear nature of the problem. The goal is therefore to calculate the values of the transformation strain and of the internal variables (*i.e* martensite volume fraction) needed to describe the current state at any material point. The *closest point projection* (CPP) approach is used and it is explained in details in the work of Qidwai and Lagoudas [68]. This kind of numerical implementation belongs to a wider class of algorithms, called *return mapping algorithms* which makes use of an elastic predictor-transformation corrector procedure and are often used within the framework of computational inelasticity [79]. In particular, a simplified version of the closest point projection method, know as the *convex cutting plane algorithm* (CCP), is used to compute the transformation strain as it evolves during the analysis; the simplification consists assuming that the transformation strain direction tensor, $\mathbf{\Lambda}$, can be defined based on its value at the previously converged iteration, which therefore enables to smooth the fully implicitly nature of the CPP scheme. The steps reported below refers to those presented in

the work of Lagoudas et al. [44]. According to the CPP algorithm, equation 2.2.2 can be written in a iterative fashion as follows

$$\boldsymbol{\varepsilon}_{n+1}^{t(k+1)} = \boldsymbol{\varepsilon}_{n+1}^{t(k)} + \Delta\boldsymbol{\varepsilon}_{n+1}^{t(k)} \tag{2.3.10}$$

where the increment in the transformation strain can be defined in the following form

$$\Delta\boldsymbol{\varepsilon}_{n+1}^{t(k)} = \Big(\xi_{n+1}^{(k+1)} - \xi_n\Big)\boldsymbol{\Lambda}^t\Big(\boldsymbol{\sigma}_{n+1}^{(k+1)}\Big) - \Big(\xi_{n+1}^{(k)} - \xi_n\Big)\boldsymbol{\Lambda}^t\Big(\boldsymbol{\sigma}_{n+1}^{(k)}\Big), \tag{2.3.11}$$

by employing the aforementioned simplification, $\boldsymbol{\Lambda}^t\Big(\boldsymbol{\sigma}_{n+1}^{(k+1)}\Big) \simeq \boldsymbol{\Lambda}^t\Big(\boldsymbol{\sigma}_{n+1}^{k}\Big)$, the previous expression reduces to

$$\Delta\boldsymbol{\varepsilon}_{n+1}^{t(k)} = \Big(\xi_{n+1}^{(k+1)} - \xi_n^k\Big)\boldsymbol{\Lambda}^t\Big(\boldsymbol{\sigma}_{n+1}^{(k)}\Big) = \Delta\xi_{n+1}^k\Lambda^t\Big(\boldsymbol{\sigma}_{n+1}^{(k)}\Big). \tag{2.3.12}$$

Therefore, the stresses can be written in the same fashion

$$\boldsymbol{\sigma}_{n+1}^{(k)} = \boldsymbol{C}_{n+1}^{(k)}\Big[\boldsymbol{\varepsilon}_{n+1} - \boldsymbol{\varepsilon}_{n+1}^{t(k)} - \boldsymbol{\varepsilon}_{n+1}^{the}\Big], \tag{2.3.13}$$

where $\boldsymbol{C}_{n+1}^{(k)}$ indicates the iterative form for the stiffness. Given any increment in the applied load or temperature, an elastic prediction is performed implying that neither the transformation strain nor the internal variable evolve

$$\boldsymbol{\varepsilon}_{n+1}^{t(0)} = \boldsymbol{\varepsilon}_n^t,\ \xi_{n+1}^{(0)} = \xi_n. \tag{2.3.14}$$

If such a prediction violets the consistency condition for transformation (2.2.5)– *i.e.,* $\Phi_{n+1}^{(0)}$ results greater than zero – the transformation correction has to employed. Over the entire correction step, the total strain and temperature are kept constant which

implies that

$$\Delta\boldsymbol{\varepsilon}_{n+1}^{(k)} = \mathbf{0},\ \Delta T_{n+1}^{k} = 0. \tag{2.3.15}$$

The increment in the stress during the transformation correction is calculated through

$$\Delta\boldsymbol{\sigma}_{n+1}^{k} = -\boldsymbol{C}_{n+1}^{k}\Big(\Delta\boldsymbol{S}\boldsymbol{\sigma}_{n+1}^{(k)} + \boldsymbol{\Lambda}_{n+1}^{t(k)}\Big)\Delta\xi_{n+1}^{(k)}. \tag{2.3.16}$$

It has to be noticed that, while the iterative correction is performed, the consistency condition (2.2.5) has to be concurrently satisfied. This requirement can be met by applying the following constraint

$$\Phi_{n+1}^{t(k)} + \Delta\Phi_{n+1}^{t(k)} = \Phi_{n+1}^{t(k+1)} \simeq 0. \tag{2.3.17}$$

This dictates a change in the internal variable which can be increased or decreased through,

$$\Delta\xi_{n+1}^{k} = -\frac{\Phi_{n+1}^{t(k)}}{A^{t}} \tag{2.3.18}$$

This expression for $\Delta\xi_{n+1}^{k}$, as well as the meaning of A^{t}, are derived in details in the work of Lagoudas et al [45, 44]. The transformation strain at the next iteration is calculated through

$$\boldsymbol{\varepsilon}_{n+1}^{t(k+1)} = \boldsymbol{\varepsilon}_{n+1}^{t(k)} + \Delta\xi_{n+1}^{k}\boldsymbol{\Lambda}_{n+1}^{t(k)} \tag{2.3.19}$$

These updated quantities are used to calculate the new stress (equation 4.27) and the new Φ_{n+1}^{k+1}. The correction step is terminated either when the consistency condition is satisfied within a certain tolerance or the limits for ξ are attained (i.e $\xi = 1$ for fully transformed martensite or $\xi = 0$ for fully austenite). The numerical implementation of the constitutive into FEA framework is outlined in Figure 2.1.

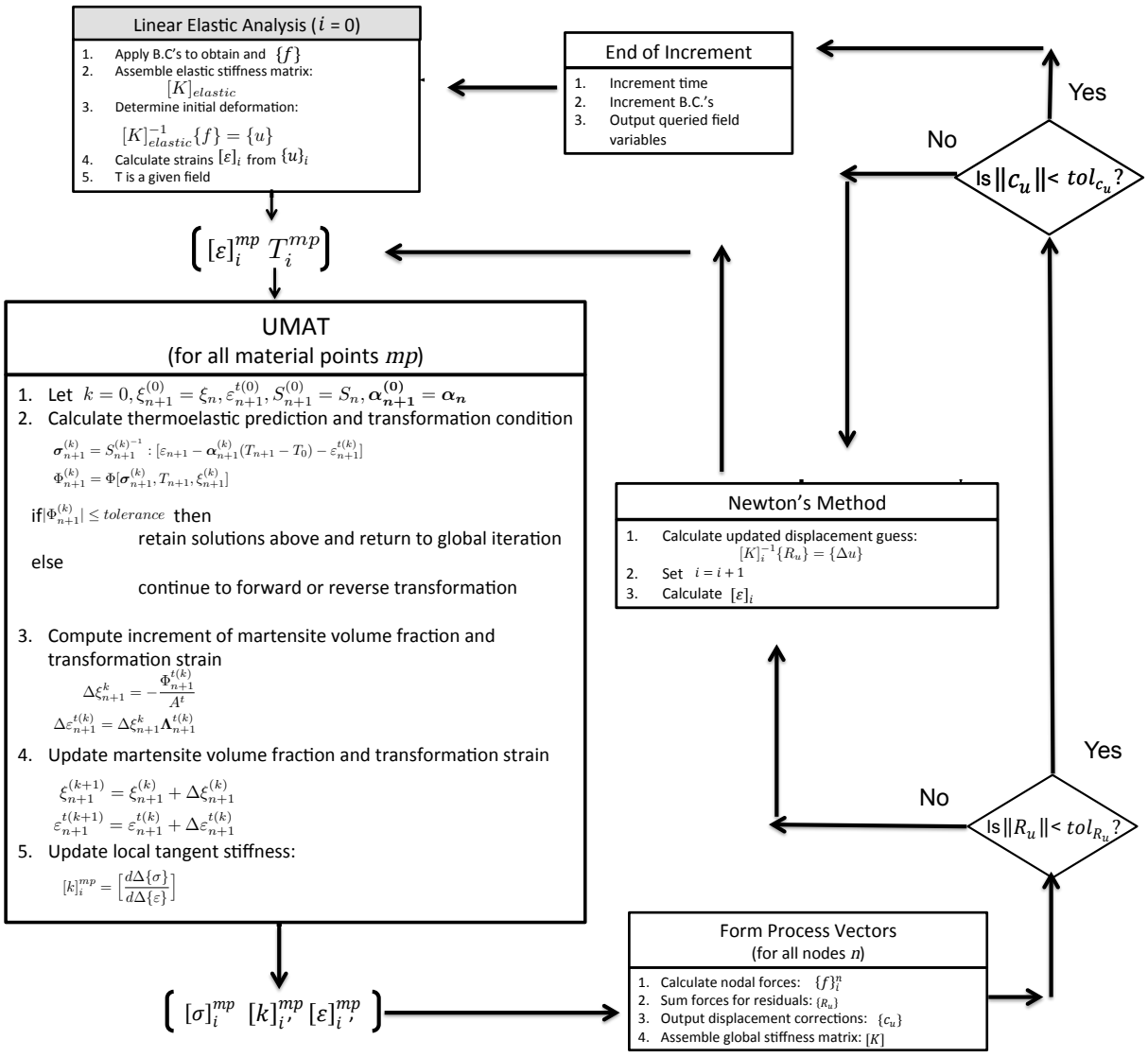

Figure 2.1: Flow chart: numerical implementation of the constitutive model

3. EFFECT OF PHASE TRANSFORMATION ON THE FRACTURE BEHAVIOR OF PSEUDOELASTIC SMAS*

In this section finite element analyses are performed to study the fracture behavior of pseudoelastic SMA initially in the austenitic phase, under nominally isothermal, plane strain, mode I loading conditions. Under monotonic increasing loading conditions a region of stress-induced martensite is formed around the crack tip where the highest concentration of stresses occurs. The initial temperature is assumed fixed at 100 ^{o}C, which is below the austenite starting temperature A_f, except if stated otherwise, therefore the constitutive model is restricted to the case of forward transformation. Although the material is assumed initially in the austenitic phase, the analysis could be applied for martensitic shape memory alloys as well. Such an analysis would only re- quire a recalibration of the model parameters. A schematic of the loading path in the temperature-stress space is provided in Figure 3.1. It is aimed to characterize the mechanical fields around a stationary crack and to investigate the fracture toughness enhancement due to transformation dissipation during quasi-static stable crack growth. Results pertaining to the influence of stress-induced phase transformation on the near-tip mechanical fields and the ratio of the far-field energy release rate to the crack-tip energy release rate are presented, showing fracture toughness enhancement in accordance with experimental observations. Moreover, the effect of plastic dissipation on the fracture resistance in SMAs is discussed.

*Part of this chapter is reprinted with permission from "On the fracture toughness enhancement due to stress-induced phase transformation in shape memory alloys" by Baxevanis, T., Parrinello, A.F., Lagoudas, D.C., 2013, International Journal of Plasticity. doi: http://dx.doi.org/10.1016/j.ijplas.2013.04.007

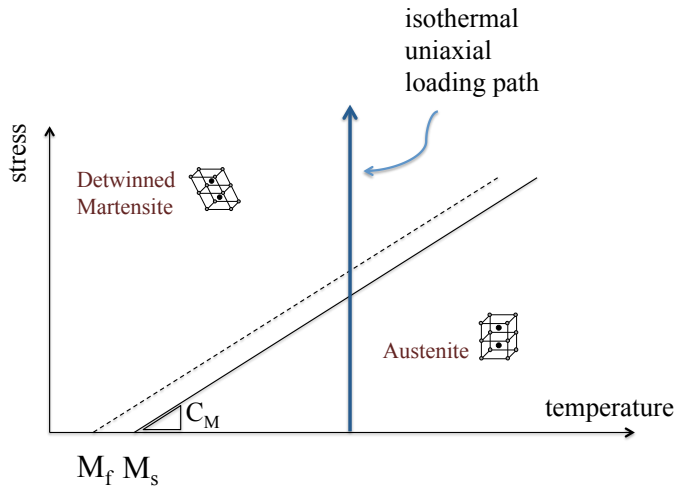

Figure 3.1: Schematic pseudoelastic loading under nominally isothermal conditions

3.1 Problem Formulation

The plane-strain crack growth for an SMA system initially in the austenitic phase is modeled under the assumption of a transformation zone small compared to the characteristic lengths of the crack configuration (see Figure 3.2). According to the boundary layer approach introduced by Rice [71], the resulting small scale transformation problem for any crack configuration can be formulated by replacing: (i) the actual configuration by a semi-infinite crack in an infinite body, and (ii) the actual boundary conditions by the requirement of an asymptotic approach to Irwin's characteristic linear elastic inverse-square-root stress/strain distribution at large distances from the crack tip. This formulation can be implemented in a large but finite region by restricting the size of the transformation zone to a small fraction of the region in order to preserve the small scale transformation condition. Coordinate systems $(x_1,\ x_2)$ and $(r,\ \theta)$ are chosen centered at the crack tip with the crack lying along $x_1 < 0$ and the faces on $\theta = \pm\pi$. Displacement boundary conditions are imposed

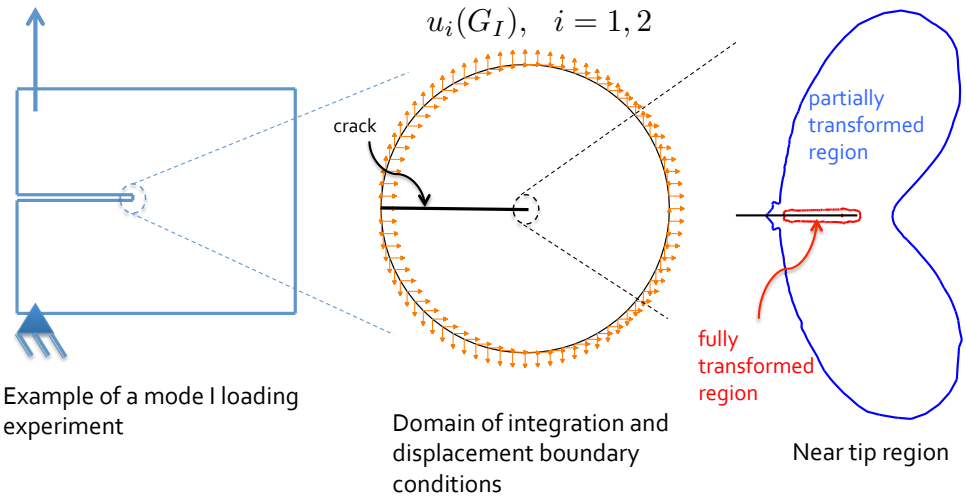

Figure 3.2: The small scale transformation assumption and the corresponding boundary value problem for a semi-infinite crack subjected to mode I loading.

on the outer boundary corresponding to the displacements associated with a linear elastic field [41]

$$u_i = G_I \hat{u}_i^I(\theta)\sqrt{\frac{r}{2\pi}}, \quad i = 1, 2, \tag{3.1.1}$$

characterized by a far-field energy release rate, G_I, corresponding to the applied mode I loading. $\hat{u}_i^I$ is a function of the polar angle θ, the Young's modulus E_A, and Poisson's ratio ν_A of austenite. These boundary conditions correspond to the displacement field in an infinite elastic isotropic medium containing a semi-infinite crack and their nature will be clarified in the next section. Moving from the boundary inwards to the crack tip, a region of partially transformed material will be first encountered and closer to the crack tip a region of fully transformed material. The incremental response of the material inside the latter, fully transformed zone is also linear elastic, and the fields are characterized by an unknown crack-tip energy release rate, $G_{I_{tip}}$.

3.2 Static Cracks

The purpose of this section is to provide a detailed description of the mechanical field close to the crack tip where the material is expected to be fully-transformed into martensite. According to the constitutive model adopted, the martensite is assumed to behave linearly elastically, therefore the stress/strain distribution can be studied by employing the principles of linear elastic fracture mechanics (LFEM). Analytical solutions have shown that, in isotropic homogenous linear elastic materials, the near-crack tip mechanical fields are characterized by an asymptotic behavior which leads to a theoretical unbounded state of stress [41, 97, 40, 98]. Therefore, it is necessary to reproduce the singular behavior of the mechanical fields which can be accomplished by using *singular collapsed elements*. The finite element mesh is designed such these special purpose elements are placed around the crack tip and equally spaced on a 15^0 basis. The rest of the grid consists of classical 8-noded isoparametric elements and a smooth transition in the element size is adopted as the outer boundary is reached (Figure 3.3). A brief overview concerning the construction of the singular elements and their properties is provided next. Results related to the mechanical fields and the region of stress-induced transformation formed around the crack are reported. The calculations are performed using the ABAQUS Unified FEA suite [1], into which the constitutive model described in Chapter 2 has been implemented as an user subroutine. The values of the material properties are chosen to conform with those of an SMA material characterized by Hartl and Lagoudas [37], listed in Table 3.1.

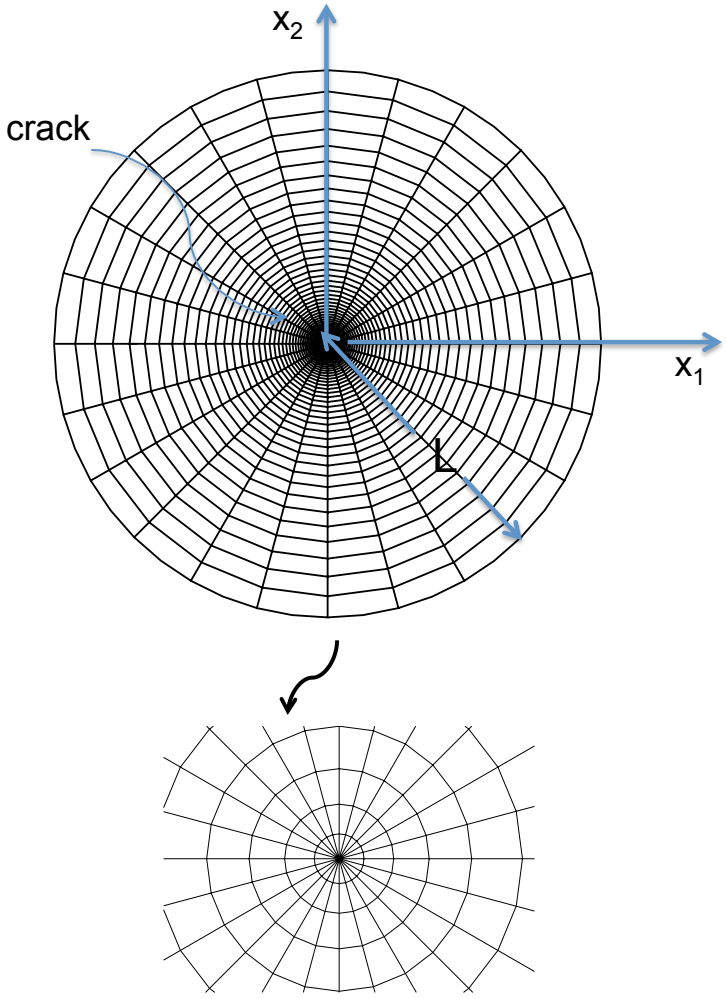

Figure 3.3: The finite element mesh used to analyze the small scale problem of a stationary crack. The mesh comprises 3120 quadratic isoparametric elements. Singular elements are placed around the crack tip at every 15^0 *From top to bottom:* Full grid – near-tip grid consisting of singular collapsed elements.

Table 3.1: Parameter used in the calculations. Material properties conformed to those of an equiatomic NiTi.

parameter	value	parameter	value
E_A (MPa)	69000	H	0.06
E_M (MPa)	38000	M_f (^{o}C)	46
ν_A	0.33	M_s (^{o}C)	48
ν_M	0.33	C_M(MPa ^{o}C^{-1})	8.7
		$n_1 = n_2$	1

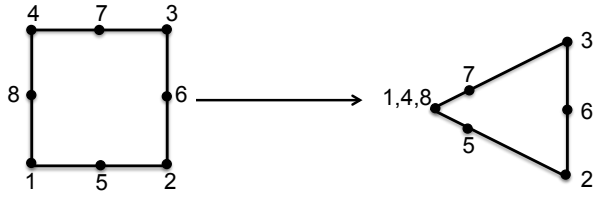

Figure 3.4: Construction of singular-collapsed elements

3.2.1 Singular Elements

First attempts in studying the mechanical fields around stationary cracks in linear elastic materials were based on the refinement of the finite element discretization close to the crack tip. It was noticed that classical isoparametric formulations could not capture accurately, within certain tolerance, the expected asymptotic behavior in the vicinity of the crack. Moreover, it turned out that this approach resulted in a significant rise of the computational costs and modeling strategies based on substructures techniques were proposed later to overcome this issue [34]. Other authors suggested solutions based on the enrichments of the classical finite element shape functions such that the singularity in the near crack tip strain field is recovered. However, a significant increase in the accuracy of the description of the crack tip

behavior was achieved when Barsoum [7] and Henshell and Shaw [38] proposed the employment of a special class of elements, the so-called *singular elements*; a detailed discussion concerning their formulation can be found in the work of Banks-Skill and Bortman [5]. In the present work, this approach has ben used to characterize the mechanical fields close to the crack tip in the region of fully-transformed martensite. The methodology needed to build such a discretization is briefly explained in the following according to the implementation adopted in ABAQUS [1]. Singular elements are constructed from eight-noded isoparametric elements by collapsing two of the opposite parallel sides such that a triangular shape is generated (Figure 3.4). The square root singularity in the stress/strain fields can be recovered by moving the midspan nodes, 5 and 7, to the quarter point location and by kinematically constraining nodes 1,4,8 to move together.

3.2.2 Near-Tip Stress-Induced Martensitic Transformation and Crack-Tip Stress Field

The transformation zone boundary and the contour plot of martensite volume fraction ξ are presented in Figure 3.5. The length parameters are normalized by

$$R_\xi = \frac{1}{3\pi}\frac{E_A G_I}{((1-\nu_A^2)\,(\sigma^{M_s})^2}, \tag{3.2.2}$$

where $\sigma^{M_s}(T) = C_M(T - M_s)$ is the stress required for initiation of transformation at a given temperature $T > M_s$. The expression used in (3.2.2) refers to the Irvin's approximation for the plastic zone around the crack tip under plain strain conditions. As a matter of fact, a similar length scale was proposed by Du and Hancock [25] for elastic-plastic materials under plane strain conditions, in which the yield stress was used instead of σ^{M_s}. In the calculations, the R_ξ-value is in between 0.9 to 1.5 times the numerically evaluated size of the transformation zone. As far as the

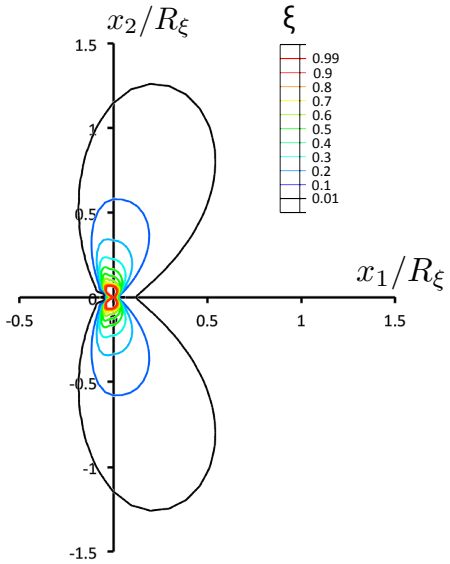

Figure 3.5: Isocurves representing the stress-induced martensite around a stationary crack

mechanical fields are concerned, the stresses close to the crack-tip, inside the region of fully-transformed elastically-deformable martensite, recover the angular distribution typical of an elastic isotropic material (Figure 3.6). In particular, the stresses values for any material point placed around the crack tip (Figure 3.7), corresponds to the classical Williams' solution which reads as follows [2]

$$\sigma_{11} = \frac{K_I}{\sqrt{2\pi r}} \cos\left(\frac{\theta}{2}\right)\left[1 - \sin\left(\frac{\theta}{2}\right)\sin\left(\frac{3\theta}{2}\right)\right] + T \tag{3.2.3a}$$

$$\sigma_{22} = \frac{K_I}{\sqrt{2\pi r}} \cos\left(\frac{\theta}{2}\right)\left[1 + \sin\left(\frac{\theta}{2}\right)\sin\left(\frac{3\theta}{2}\right)\right] \tag{3.2.3b}$$

$$\sigma_{12} = \frac{K_I}{\sqrt{2\pi r}} \cos\left(\frac{\theta}{2}\right)\sin\left(\frac{\theta}{2}\right)\cos\left(\frac{3\theta}{2}\right) \tag{3.2.3c}$$

$$\sigma_{33} = \nu(\sigma_{11} + \sigma_{22}) \tag{3.2.3d}$$

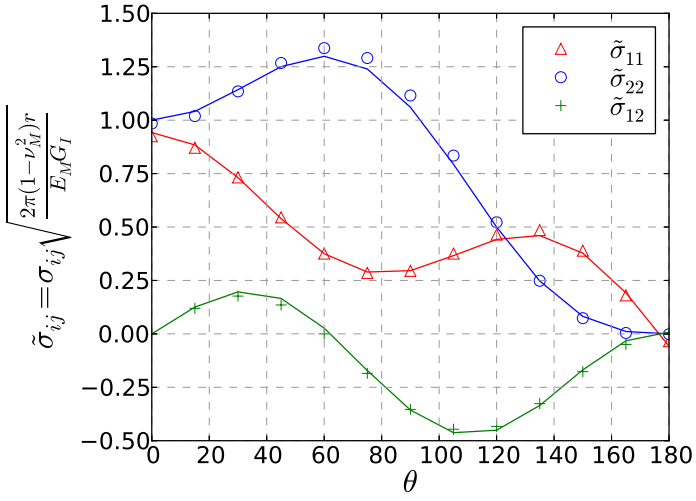

Figure 3.6: Angular variation of stress components near the crack tip. The markers are numerical results for the SMA and the dashed lines are the result for an isotropic elastic material. The numerical results plotted are for all integration stations within the radial distance $5 \times 10^{-3} R_\xi < r < 7 \times 10^{-3} R_\xi$. The $1/\sqrt{r}$ radial dependence has been accounted for within the normalization.

In (3.2.3) K_I represents the stress intensity factor which is a parameter introduced to characterize the near-crack tip state according to the geometry and loading conditions. However, for linear elastic material the stress intensity factor can be expressed in terms of the energy release rate according to the following relation:

$$G_i = \frac{K_i^2}{E^*} \tag{3.2.4}$$

where E^* assumes the values of $E/(1-\nu^2)$ and E for plain strain and plane stress respectively. It has to be noticed that in Figure 3.6 the angular distribution of the stresses has been normalized by using the value of the applied far-field G_I and by taking into account the $1/\sqrt{r}$ dependence. In LFEM the energy release rate coincides

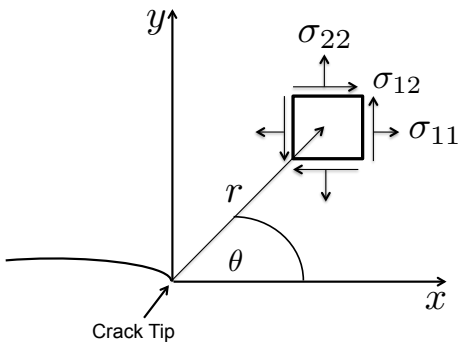

Figure 3.7: Stresses acting on a material element in the vicinity of the crack tip

with the $J-integral$ thus its properties can be recalled. Under plane strain and small scale transformation conditions and assuming that any non-proportional loading effects near a stationary crack can be neglected, the path-independence of the J-integral [71] implies that the crack-tip energy release corresponds to that applied on boundary (equation 3.1.1). Moreover, it has to be remarked that, in order to fully describe the distribution of σ_{11}, the Williams's expansion has to be written up to the second term. Such a term, the so called $T-stress$, refers to a constant stress acting parallel to the crack plane, compressive in this case, and can be estimated as $\sigma_{22}(0^0)-\sigma_{11}(0^0)$. This constant term has to be introduced in order to account for the constraints due to the transformation strains generated ahead of the crack tip. However, Rice [69] showed that, for the case of in-plane loading under small scale yielding (*i.e.,* small scale transformation), the presence of the $T-stress$ does not affect the $J-dominance$ of the mechanical fields. Therefore, the crack tip behavior can be uniquely described by the energy release rate G_I. Moreover, numerical calculations have shown that the value of $T-stress$ becomes smaller for material systems with lower maximum transformation strain.

3.3 Crack Propagation

Crack growth is presumed to proceed at a critical level of the crack-tip energy release rate, denoted as G_{I_c}, and considered to be a constant material property. There are indications based on both numerical calculations and experimental evidence suggesting that the contribution of plastic dissipation on the overall fracture resistance of SMAs might be a small fraction of the respective contribution of energy dissipation due to phase transformation. Finite element analysis performed by Baxevanis et al. [8] showed that the size of the crack-tip plastic zone is an order of magnitude smaller than the one anticipated in conventional elastic-plastic materials. This result is due to stress relaxation associated with stress-induced phase transformation occurring around the crack tip which therefore tends to inhibit the material to undergo plastic yielding. Moreover, experimental evidence of cleavage fracture and river markings appearing consistent with markings from traditional brittle intermetallic alloys in binary NiTi systems containing semi-coherent precipitates was reported in the work of Gall et al.[30]. Based on those findings, it seems reasonable that the length scale of the fracture process zone should be small enough to ensure the validity of both the point fracture criterion and the constitutive law used in the analysis presented in the previous sections; a discussion on the validity of a point fracture toughness criterion can be found in the work of Carka and Landis [49, 19]. The Virtual Crack Closure Technique is employed in the analysis for computing the crack-tip energy release rate and it is explained in the following section. A finite element mesh of four-noded, isoparametric elements is designed with crack-tip elements small compared to the circular finite domain (Figure 3.8). For this temperature, which is below the austenitic-start temperature A_s, the extent of reverse phase transformation occurring in the wake of the advancing crack is expected to be none or negligible.

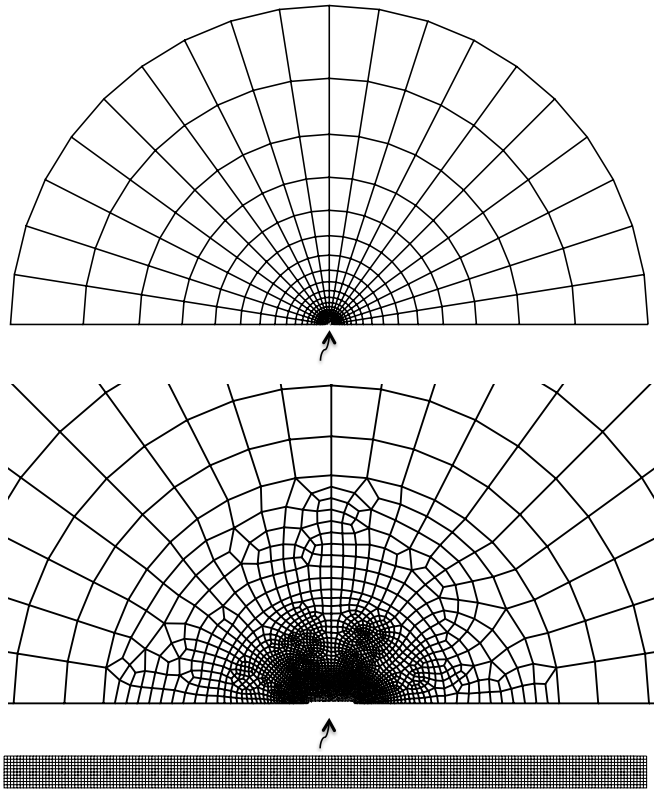

Figure 3.8: The finite element mesh used to analyze the small scale growth problem. The mesh comprises 10078 quadrilateral elements. Crack growth by nodal release is permitted to occur over a span of 180 nodes. *From top to bottom:* Full grid – near-tip grid – refined grid along the crack path.

3.3.1 The Virtual Crack Closure Technique

The Virtual Crack Closure Technique (VCCT) is a method used within the framework of finite element analysis to compute strain energy release rates in elastic isotropic solids. Pioneering works are attributed to Rybicki and Kanninen [75] who proposed the use of VCCT to calculate stress intensity factor values for two dimensional cracked bodies. Shivakumar et al. [76] were able to study surface cracked plates by using the same approach and therefore to extend the framework to three dimensional bodies. It should be mentioned that the VCCT can be classified as an indirect procedure, as pointed out by Fawaz [28], since the stress intensity factor, K_i, is not directly computed while it is extrapolated through expression 3.2.4. Furthermore, it has been extensively employed to study delamination in composite materials and debonding is sandwich structures [43]; however few researchers have relied on it to analyze progressive crack growth [99]. The VCCT has been historically identified as an extension of the classical crack closure method based on the Irwin's integral [41]. This conservation integral states that the work needed to extend a crack of length a of an infinitesimal amount, Δa, is the same as that needed to close it of the same length which implies that the system evolves in a self-similar fashion ($i.e$ $K(a) \simeq K(a + \Delta a)$). As far as two-dimensional problems are concerned, the Irwin's integral for mode I loading conditions (Figure 3.9) reads as follows

$$G_I = \lim_{\Delta a \to 0} \frac{1}{2\Delta a} \int_0^{\Delta a} \sigma_{22} \left(\Delta a - r, 0\right) u_2 \left(r, \pi\right) \, dr \tag{3.3.5}$$

where σ_{22} is the stress acting perpendicular to the crack plane ahead the crack tip and u_2 is the crack opening displacement ($i.e$ COD) measured at an infinitesimal distance, Δa, behind the crack tip. Within the context of finite element (3.3.5) can

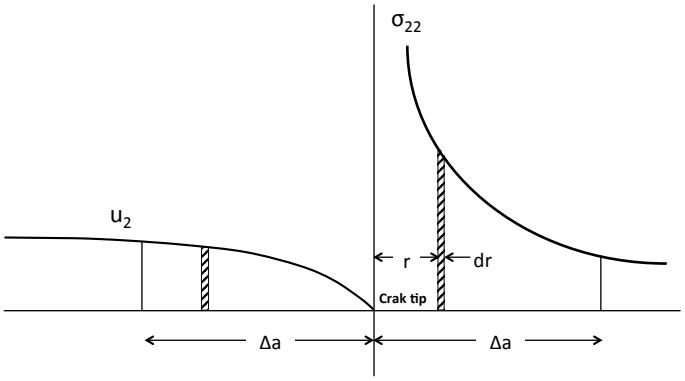

Figure 3.9: Schematic of Irwin's crack closure integral

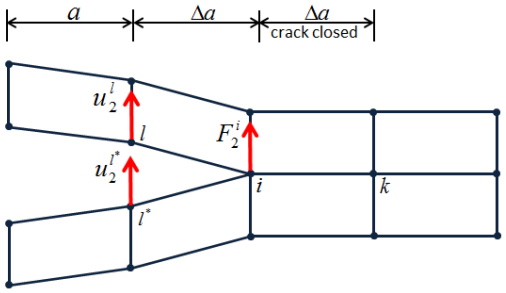

Figure 3.10: VCCT for four-noded elements.

be reduced to the product of nodal forces on the crack front and nodal displacements behind the crack tip. For the case of two-dimensional four noded elements (Figure 4.4), as employed in the present analysis, the energy release rate is computed in one step procedure as

$$G_{I_{tip}} = -\frac{1}{2\Delta a} F_2^i (u_2^l - u_2^{l^*}), \tag{3.3.6}$$

where F_2^i indicates the perpendicular to the crack plane nodal force at the tip and u_2^l, $u_2^{l^*}$ represent the opening displacement of the upper and lower crack surfaces,

respectively [43]. The method therefore assumes that: (i) a crack extension of Δa from $a+\Delta a$ (node i) to $a+2\Delta a$ (node k) does not significantly alter the state at the crack tip (Figure 4.4), and (ii) the energy released when the crack is extended by Δa from $a+\Delta a$ to $a+2\Delta a$ is identical to the energy required to close the crack between location i and k (Figure 4.4). The former assumption is justified for a constitutive material behavior that results in a linear, elastically-deformed material region surrounding the crack tip which, as reported previously, in which the mechanical fields are uniquely described by the energy release rate. The latter statement relies on the approximation that the difference between the energy needed to extend and close the crack of the same amount is locally negligibly affected by the stress-induced phase transformation. A finite element mesh of four-noded, isoparametric, quadrilateral elements is designed with crack-tip elements small compared to the circular finite domain (Figure 3.8). It will be shown that the as the crack growths, a region of fully-transformed elastically-deformable martensite progressively forms around the crack tip which therefore supports the use of this method based on the adopted assumptions.

3.3.2 Fracture Toughness Predictions

The contour plot of martensite volume fraction, ξ, close to steady state conditions is presented in Figure 3.11. The crack has advanced approximately five times the size of the transformation zone at initiation of crack propagation before reaching nominally steady state conditions. Clearly, the zone boundary between fully transformed and untransformed regions occurs over a diffuse region (zone of partial transformation). The height of the fully transformed zone exhibits a peak at the initial stage of crack growth. Such a peak was reported in the work of Stump and Budiansky [83], in which, however, similarly to Yi et al. [102, 103], the simplifying assumption of su-

percritical transformation, *i.e.*, either no transformation or complete transformation once a level of stress is achieved at a material point, was utilized. Numerical results

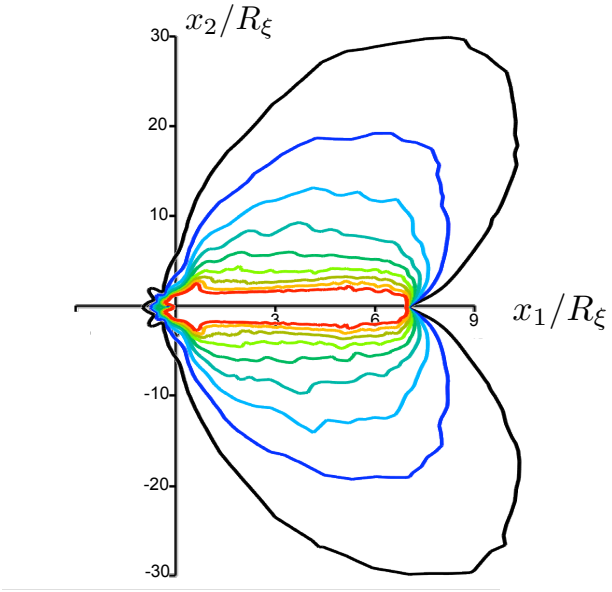

Figure 3.11: Transformation zone boundary and contour plot of the martensite volume fraction ξ close to steady-state conditions

for a static crack using collapsed elements to account for the singular behavior of the stress field in the vicinity of the crack tip suggest that at initiation of crack propagation the crack-tip stress field is indeed equivalent to the asymptotic stress field for a linear isotropic elastic material (Figure 3.6). As the crack advances at a constant level of the crack-tip energy release rate, the crack-tip mechanical fields should remain unchanged, identical to those at initiation of crack propagation. However, a discretization error is expected, especially since non-singular crack-tip elements are used in the calculations. To test the accuracy of the calculations, the opening displacement of the crack surface $\delta^{a+\Delta a}$ $(= u_2^l - u_2^{l^*}$, see Figure 4.4) is plotted during

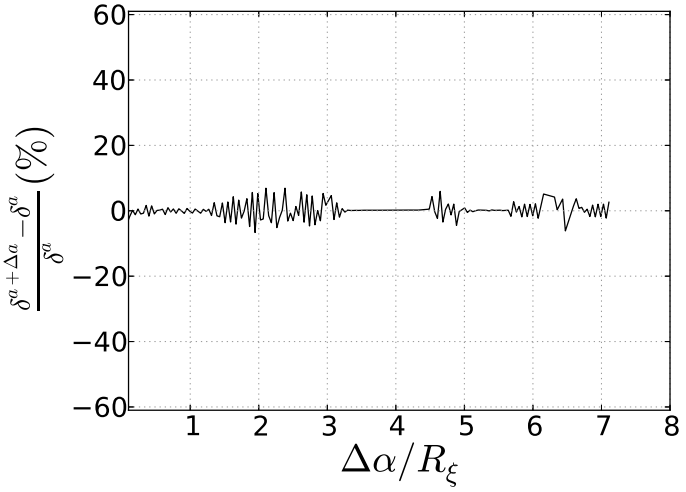

Figure 3.12: Relative change of the opening displacement of the crack surface $\delta^{a+\Delta a}$ $(= u_2^l - u_2^{l^*}$, see Figure 4.4) during crack growth.

crack growth in Figure 3.12. A relative error of up to 7% is found. This discretization error is reduced for crack-tip elements of smaller size. However, the effect on the overall mechanical response is negligible and therefore this error in approximating the singular mechanical fields in the vicinity of the crack tip is considered acceptable for the purpose of the calculations presented below.

The dependence of the fracture toughness enhancement associated with stress-induced transformation, as given by the ratio G_I/G_{Ic}, on the thermomechanical material properties and temperature is examined next. Dimensional analysis dictates that the relative toughening ratio, G_I/G_{I_c}, will be dependent on the following dimensionless parameters

$$\frac{E_A H}{\sigma^{M_s}}, \frac{M_s - M_f}{T - M_s}, \frac{E_M}{E_A}, \nu.$$

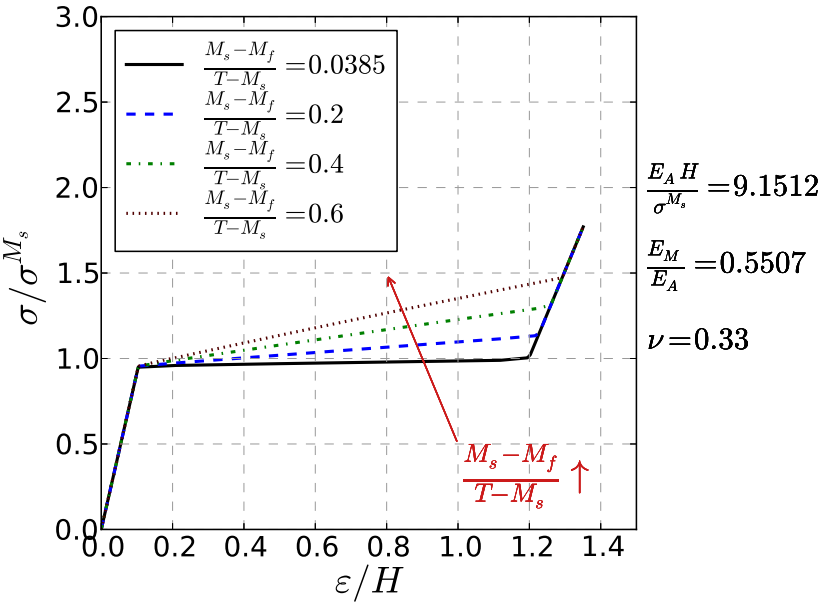

Figure 3.13: Uniaxial stress–strain response for a range of the non-dimensional parameters $(M_s - M_f)/(T - M_s)$. The stresses are normalized by the stress required to initiate forward transformation,σ_s^M and the strain by the maximum transformation strain,H

Note that $\frac{M_s-M_f}{T-M_s} \geq 0$ since $M_f \leq M_s$ and the material is assumed initially in the austenitic phase ($T > M_s$). $E_A H/\sigma^{M_s}$, which has been identified as the most significant parameter in all transformation toughening models, is the ratio of the transformation strain to the characteristic elastic strain in the material. If rearranged as $\sigma^{M_s} H/\left[\left(\sigma^{M_s}\right)^2/E_A\right]$, it can also be interpreted as the ratio of the characteristic level of dissipated to stored energy in the material. $(M_s - M_f)/(T - M_s)$ is related to the difference between the martensitic-start σ^{M_s} and martensitic-finish σ^{M_f} stresses through $(M_s - M_f)/(T - M_s) = (\sigma^{M_f} - \sigma^{M_s})/\sigma^{M_s}$ and is indicative of the transformation hardening (Figure 3.13). The parameters chosen to vary are $E_A H/\sigma^{M_s}$, $(M_s - M_f)/(T - M_s)$, and E_M/E_A since Poisson's ratio, ν, is approximately the

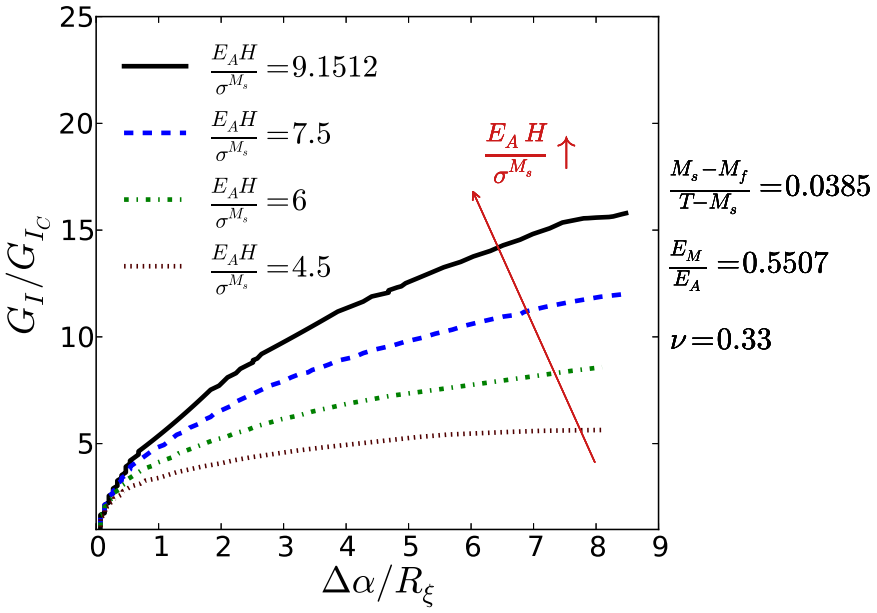

Figure 3.14: Fracture toughness enhancement, G_I/G_{Ic}, vs normalized crack extension $\Delta a/a$, for a range of relative maximum transformation strain, E_AH/σ^{M_s}. The black solid line corresponds to the material of Table 3.1. The toughness enhancement increases with increasing relative maximum transformation strain, E_AH/σ^{M_s}.

same for most SMA material systems. As shown in Figure 3.14, the toughness enhancement increases monotonically as the relative maximum transformation strain, E_AH/σ^{M_s}, increases. Larger relative maximum transformation strains imply that the material can dissipate more energy which in turn implies higher steady state fracture toughness. It is also shown that the toughness enhancement decreases with increasing levels of transformation hardening (Figure 3.15). Increasing levels of transformation hardening induce higher stresses in the material which are required to reach given levels of martensite volume fraction. This in turn impedes transformation near the crack tip and reduces the level of transformation toughening. Finally, the effect of the ratio of the Young's moduli E_M/E_A on the fracture toughness is presented in

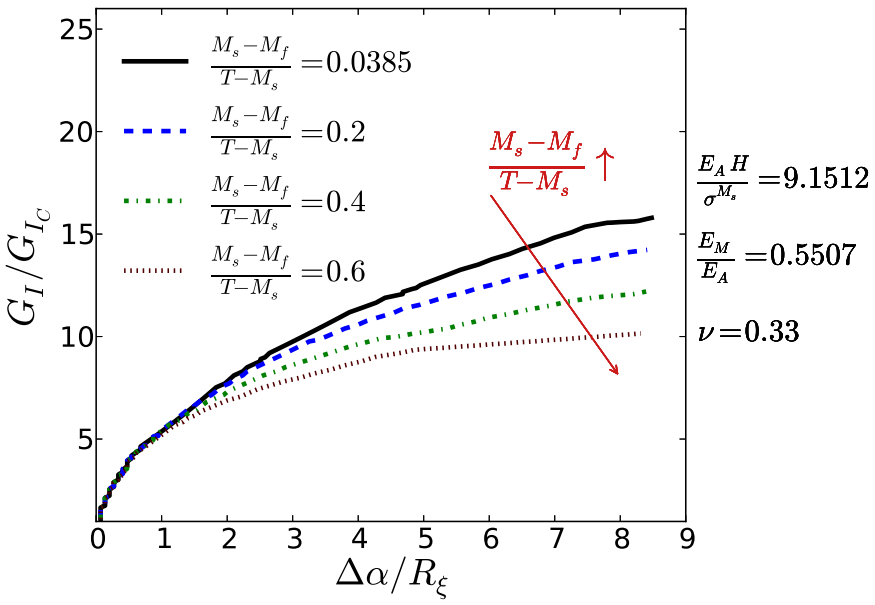

Figure 3.15: Fracture toughness enhancement, G_I/G_{Ic}, vs normalized crack extension $\Delta a/a$, for a range of the non-dimensional parameter $(M_s - M_f)/(T - M_s)$. The black solid line corresponds to the material of Table 3.1. The toughness enhancement decreases with increasing transformation hardening.

Figure 3.16. The smaller the ratio E_M/E_A, the smaller the toughening effect. This should be attributed to the fact that smaller ratios E_M/E_A lower the stress levels close to the crack tip restricting the extent of transformation for given values of the loading parameter. Thus, the energy dissipated due to phase transformation decreases and so does the level of toughness enhancement. This result is the exact opposite of that obtained by Freed et al. [29] using a cohesive zone model and the analytical result of Yi and Gao [102], in which the level of toughness enhancement was found to decrease with increasing ratios E_M/E_A. As temperature increases, the values of all the non-dimensional parameters that are temperature dependent, *i.e.*, $E_A H/\sigma^{M_s}$ and $(M_s - M_f)/(T - M_s)$, decrease. However, decreasing values of

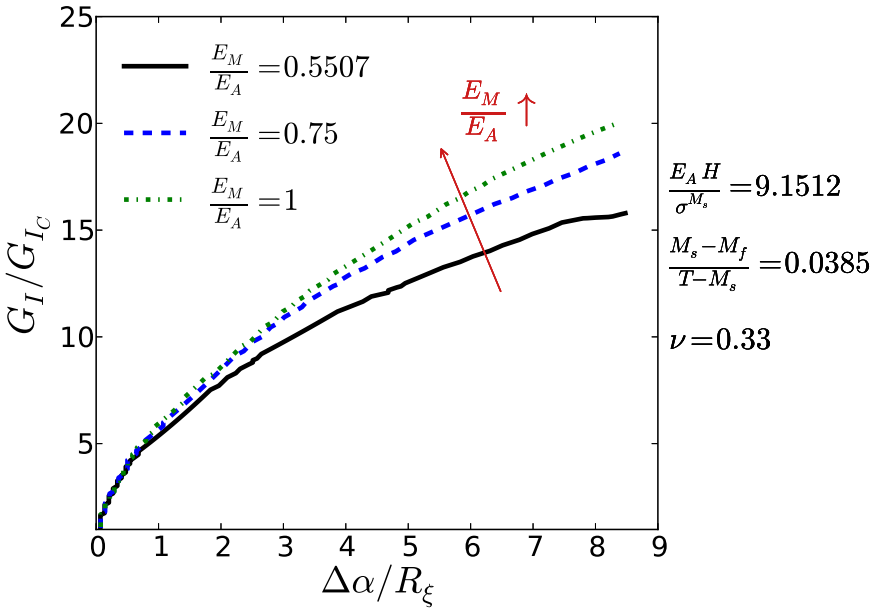

Figure 3.16: Fracture toughness enhancement, G_I/G_{Ic}, vs normalized crack extension $\Delta a/a$, for a range of ratios of Young's moduli, E_M/E_A. The black solid line corresponds to the material of Table 3.1. The toughness enhancement increases with increasing ratio $E_M/E_A \leq 1$.

$E_A H/\sigma^{M_s}$ yield lower levels of transformation-induced toughness enhancement, while decreasing values of $(M_s - M_f)/(T - M_s)$ have the opposite effect. Therefore, it is instructive to examine the effect of temperature on the toughening response. As it can be seen in Figure 3.17, increasing values of temperature result in lower levels of toughness enhancement.

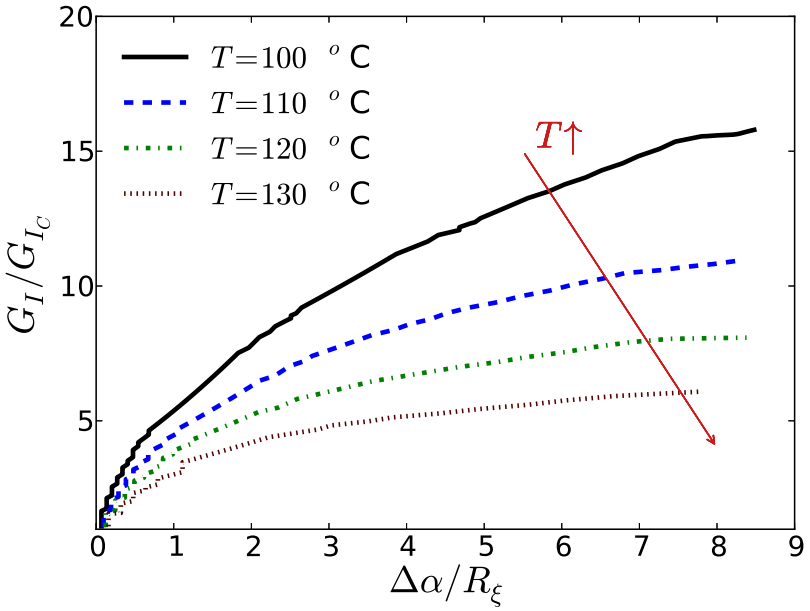

Figure 3.17: Fracture toughness enhancement, G_I/G_{Ic}, vs normalized crack extension $\Delta a/a$, for a range of temperatures, T. The material parameters listed in Table 3.1 are used in the calculations. The toughness enhancement decreases with increasing temperature, T.

3.4 Effect of Plastic Deformation on the Fracture Resistance of SMAs

In this section, the material constitutive behavior is extended to account for plastic deformation and numerical simulations are carried out to gain an insight into the effect of the associated plastic dissipation on the fracture toughness enhancement.The constitutive material behavior chosen is that described in Hartl and Lagoudas [37] which exhibits a stress-strain response of the type presented in Figure 3.18. The model parameters used in the calculations to describe plastic deformation are those reported in their work (Table 3.2) and crack growth is modeled using a Cohesive Zone Model. Moreover, it has to be mentioned that the austenitic phase is not expected to undergo plastic yielding since the operational temperatures are lower than A_f (Figure 3.19).

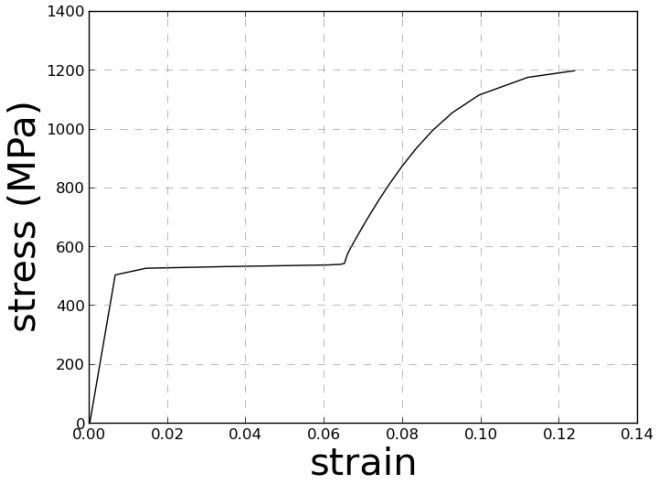

Figure 3.18: Stress-strain response for NiTi system characterized by Hartl and Lagoudas [37].

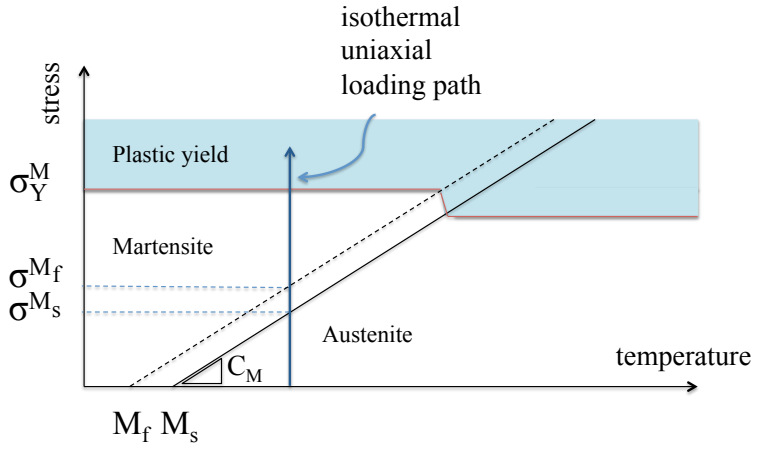

Figure 3.19: Stress–temperature phase diagram for SMA undergoing plastic yielding in the martensitic phase at temperatures below A_f.

Table 3.2: Parameter used in the calculations. Material properties conformed to those of an equiatomic NiTi undergoing plastic yielding.

parameter	value	parameter	value
E_A (MPa)	69000	H	0.06
E_M (MPa)	38000	M_f (^{o}C)	46
ν_A	0.33	M_s (^{o}C)	48
ν_M	0.33	C_M(MPa ^{o}C^{-1})	8.7
$n_1 = n_2$	1	σ_Y^M(MPa)	500

3.4.1 Cohesive Zone Model

The cohesive zone model (CZM) is employed to phenomenologically model the separation between the crack surfaces when it occurs within a finite fracture process zone (Figure 3.20) in which the material experiences progressive accumulation of inelastic deformation prior of local failure [62] and closure tractions act between the crack surfaces. Therefore, the crack tip behavior is not anymore described by only one parameter, namely G_{I_c}, as it has been previously adopted in the VCCT approach.

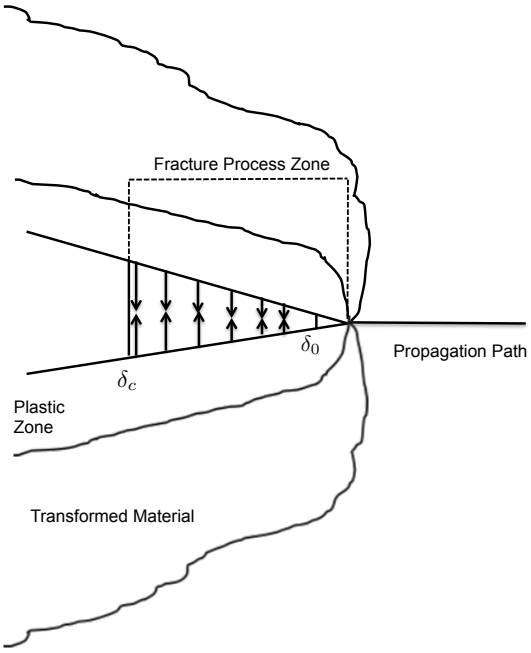

Figure 3.20: Schematic of a typical fracture process zone in SMA with a growing crack under mode I loading conditions

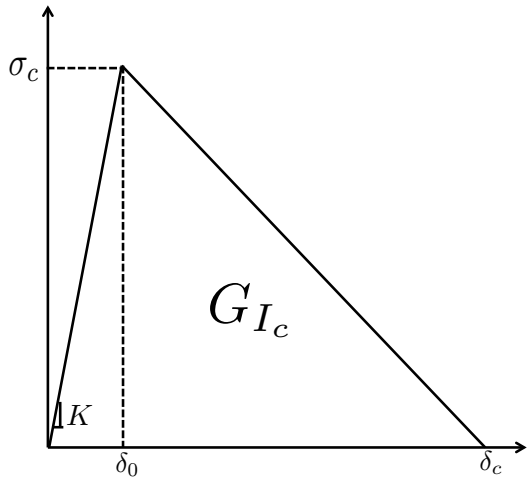

Figure 3.21: Bilinear traction separation law

Crack growth is modeled by placing a discrete layer of *cohesive elements* along the path where the crack tip is expected to progress and their constitutive response is such that they obey a traction-separation law (TSL). An interfacial potential is usually assumed to derive the relation between the tractions acting on the surfaces and the associated displacement [60]. The introduction of the CZM is historically attributed to Dugdale [26] and Barenblatt [6] and since then researchers have used this approach to study crack propagation in a variety of material systems under static [90, 91, 92] and dynamic [78, 77, 18, 101, 93] loading conditions by means of different TSL [54]. In this study a bilinear TSL, as it was proposed by Geubelle and Baylor [32], is employed (Figure 3.21). The interface is assumed to respond linear-elastically, with stiffness K (*i.e.,* penalty stiffness) until the cohesive strength, σ_c, is reached after which a linear softening behavior occurs. When the crack surfaces are displaced of an amount equal to δ_c no more cohesive tractions act in the interface meaning that the critical fracture toughness, G_{I_c} (*i.e.,* work of separation), has been reached. It has been well established that two of the three parameters can be used to completely characterize the TSL through the following relation

$$G_{I_c} = \frac{1}{2}\sigma_c\delta_c \tag{3.4.7}$$

The crack tip is assumed to be within the active fracture process zone, however a unique location cannot be identified and its choice is of crucial importance to correctly model the crack propagation process. Here, the advancing crack-tip is assumed to be located at the element that has reached the critical separation length $\delta_c = 2G_{I_c}/\sigma_c$. A fine spatial mesh discretization is necessary to reproduce the length scale of the fracture process zone, which therefore results in a significant increase in the computational costs [24]. The characteristic length of the element has to be of

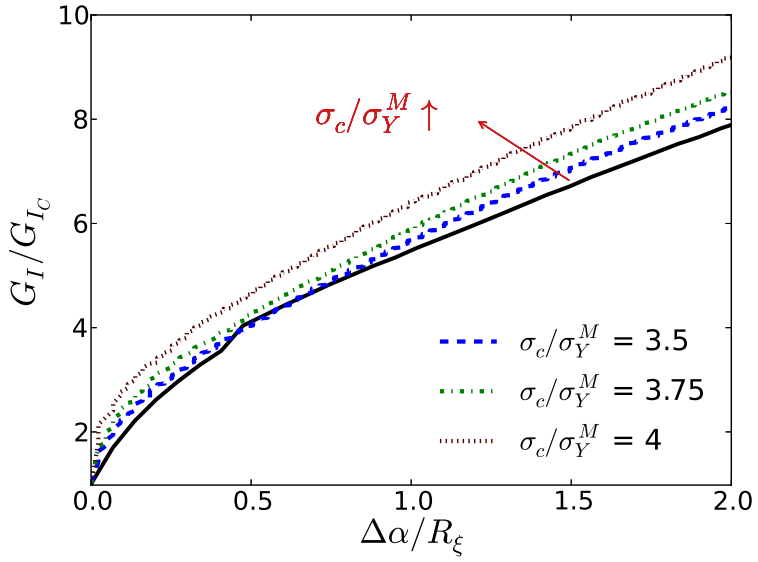

Figure 3.22: Resistance curves obtained by the CZM that account for plastic deformation for different values of the ratio σ_c/σ_Y^M. The resistance curve, denoted as a solid line, obtained by the VCCT is included for comparison purposes.

the same order of magnitude of δ_c to provide a realistic representation of the fracture process zone and ensure meaningful results and numerical convergence. The choice of the penalty stiffness, is also important in constructing the TSL since high values may lead to unexpected stress oscillations which weak the numerical convergence while small values result in an over-compliant system [89].

3.4.2 Fracture Toughness Predictions

Crack growth resistance curves at $T = 100$ ^{o}C for a range of the ratio σ_c/σ_Y^M, where σ_Y^M is the yield stress of martensite, are presented in Figure 3.22. The toughening effect obtained for $\sigma_c/\sigma_Y^M = 3.5$ is only slightly higher than the one obtained for the constitutive law that does not account for plastic deformation. The effect of plastic dissipation on the fracture resistance increases for higher values of σ_c/σ_Y^M.

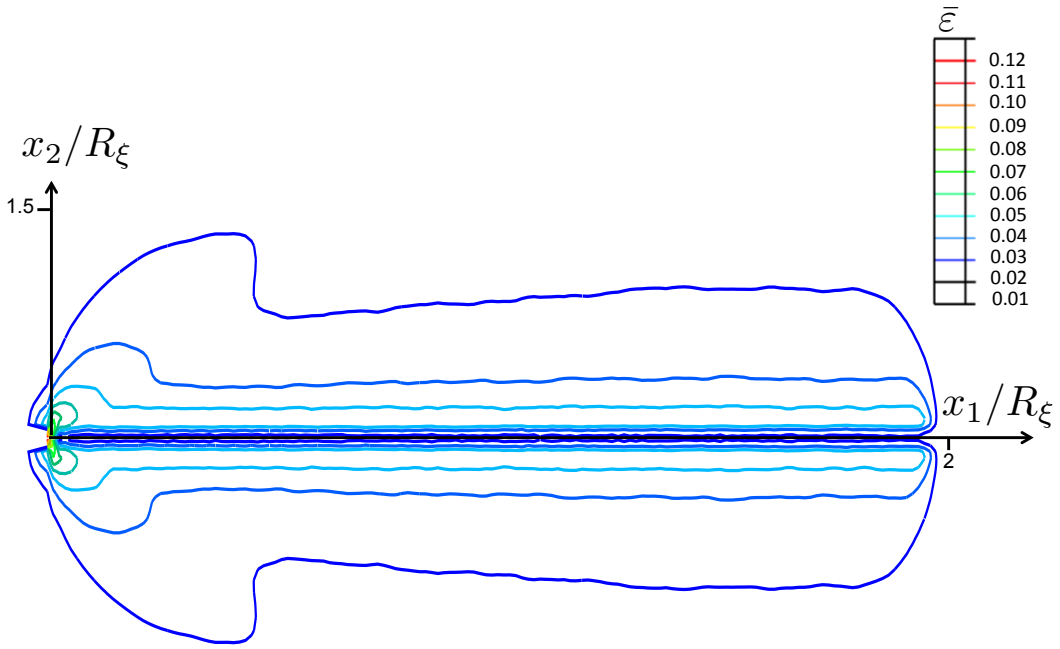

Figure 3.23: Plastic zone developed during crack propagation for the case of $\sigma_c/\sigma_Y^M = 3.5$

As explained in the work of Tvergaard Hutchinson [90], this should be readily understood in terms of the traction which develops directly ahead of the crack tip in a fully-developed plane-strain plastic zone. For a line crack with no process zone, Rice et al. [70] have shown that the traction σ_{22}/σ_Y acting on the plane ahead of tip in the plastic zone in conventional elastic-plastic materials is greater than 2.97; this value being approximative of an elastic-perfectly plastic material. Thus, for critical strengths σ_c in the proximity of this value, the crack initiates and advances without permitting a fully developed plastic zone to form. Plastic dissipation is then small compared to the work of fracture process and energy dissipated due to phase transformation. Plastic dissipation becomes significant for the fracture resistance only when a fully developed plastic zone can form. A quantitative determination of the actual effect of plastic deformation on the fracture toughening of SMAs is a very

difficult task that relies heavily on both experimentation and constitutive modeling. The traction-separation parameters σ_c and G_{I_c} are phenomenological parameters that should be chosen to give best fit of crack growth experimental data. The fitting process requires an analysis of the reference specimen used to generate the resistance curve data with iteration on both σ_c and G_{I_c}. Only, then, assuming the traction-separation law is capable of representing the fracture process in a phenomenological sense, the effect of plastic dissipation on the fracture resistance can be evaluated. In Figure 3.23 the effective plastic strain generated as the crack tip progresses is plotted. The unit axes are normalized by the size of the transformation zone at initiation of crack propagation (3.2.2). It can be seen that the plastic zone developed during crack propagation, at least for relatively small ratio of cohesive strength over the yield stress, occupies a small portion around the crack surfaces being suppressed by the surrounded transformation zone. Therefore it can be assume to be collapsed into a point which supports the use of the fracture point criterion used within the VCCT.

4. EFFECT OF THERMO-MECHANICALLY-INDUCED PHASE TRANSFORMATION ON THE CRACK DRIVING FORCE

In this section the effect of thermo-mechanically-induced phase transformation on the driving force for crack growth in SMAs is analyzed via the finite element method. The material is assumed to be initially in the austenitc state and the constitutive response to be that described by the model presented in Chapter II. The boundary value problem concerns a center-cracked plate subjected to a thermal cycle under isobaric conditions (Figure 4.1). It is aimed to describe the examine the evolution of the crack-tip energy release rate throughout the thermal cycle and its sensitivity on characteristic non-dimensional parameters.

4.1 Problem Formulation

The analysis is performed on an infinite SMA plate containing a central crack of length $2a$ subjected to in-plane uniform uniaxial tensile stress at infinity, σ_∞, in the direction perpendicular to the crack axis, under temperature variations (Figure 4.2). A system of co-ordinates (x_1, x_2) is taken such as the origin lies at the center of the crack and the x_1-axis is extending along the line of the crack. Due to the mode I symmetry of the problem only the upper quarter plane is analyzed. A finite element mesh of eight-noded, isoparametric quadrilaterals elements is designed for the analysis (Figure 4.3) with the near-crack tip finite element characteristic length thousand times smaller than the crack length. The mechanical loading is first applied at a constant nominal temperature, T_h, which is assumed greater than the austenitic-finish temperature, A_f, so that the material is initially in the austenitic phase. The resulting uniaxial tensile stress at infinity, σ_∞, is assumed sufficiently smaller than the stress required for initiation of martensitic transformation, $\sigma^{M_s} = C_M(T_h - M_s)$,

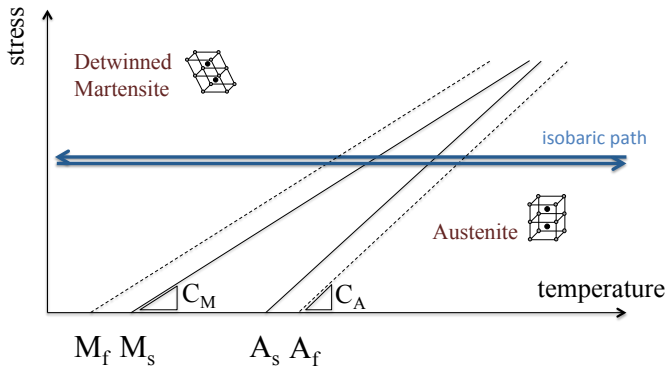

Figure 4.1: Stress–temperature phase diagram. An isobaric loading path.

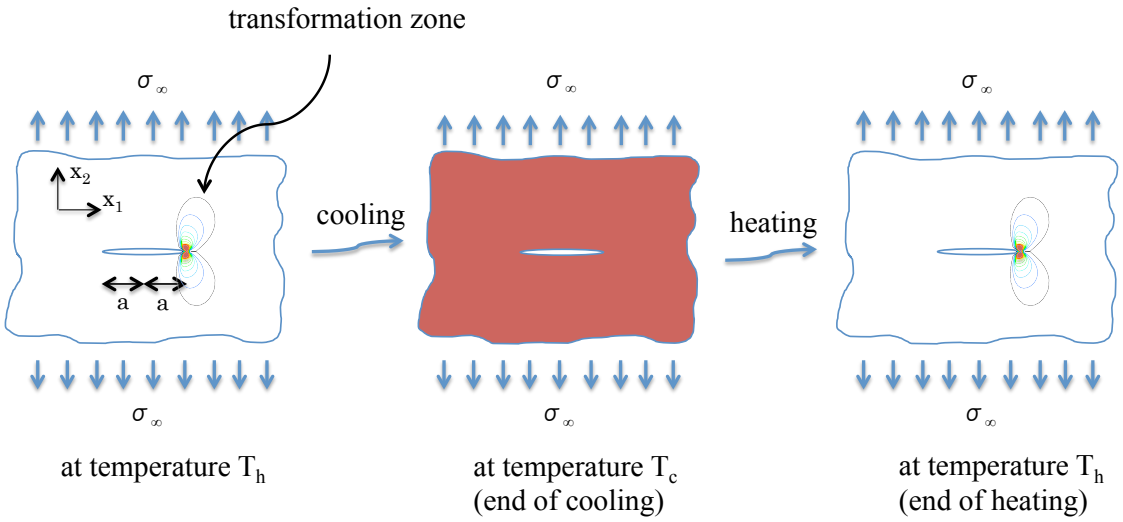

Figure 4.2: Boundary value problem for an infinite center-cracked SMA plate subjected to a thermal cycle under isobaric loading conditions. The region of fully transformed material is represented with the red color.

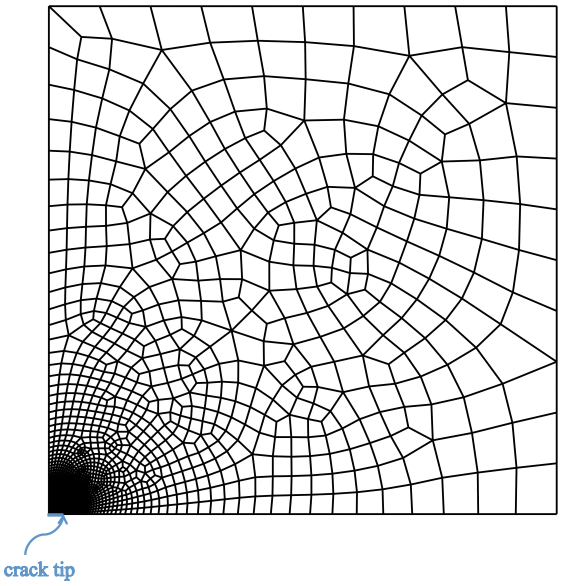

Figure 4.3: Computational grid used in the calculations. The mesh comprises 11317 eight-noded elements. A mesh refinement is performed in the vicinity of the crack tip.

at the given temperature T_h, so that small scale transformation conditions apply, according to which the size of the transformation zone is small compared to the crack length $2a$. Moving from the boundary inwards to the crack tip, a region of partially transformed material will be first encountered and closer to the crack tip a region of fully transformed material. Then the temperature is cycled between T_h and a temperature T_c, which is assumed lower than the martensitic-finish temperature, M_f, to ensure that eventually the whole material is transformed from austenite to martensite at the end of cooling. The incremental response of the material inside the fully transformed zone surrounding the crack tip at all times is linear elastic, and the fields are characterized by an unknown crack-tip energy release rate, G_I.

The VCCT is employed in the analysis for computing the crack-tip energy release rate, G_I [75, 43, 99]. In the case of the two-dimensional eight-noded elements placed

Table 4.1: Values of the non-dimensional parameters used in the numerical calculations.

parameter	value	parameter	value
$\frac{E_A H_{sat}}{\sigma_\infty}$	4	ν_M	0.33
$k\sigma_\infty$	6.25	$\frac{\nu_M}{\nu_A}$	1
$\frac{C_M(A_s-M_s)}{\sigma_\infty}$	1	$\frac{E_M}{E_A}$	0.75
$\frac{C_M(A_f-A_s)}{\sigma_\infty}$	1		
$\frac{C_M(M_s-M_f)}{\sigma_\infty}$	1		
$\frac{C_M}{C_A}$	1		

in the crack front, the energy release rate is computed in one step procedure as

$$G_I = -\frac{1}{2\Delta a}(F_2^i(u_2^l - u_2^{l^*}) + F_2^j(u_2^m - u_2^{m^*})), \tag{4.1.1}$$

where F_2^i and F_2^j indicate the perpendicular to the crack plane nodal force at the tip and at the mid-side node in front of the crack, respectively. Also, u_2^l, $u_2^{l^*}$ and u_2^m, $u_2^{m^*}$ represent the opening displacement of the upper and lower crack surfaces at the two nodes placed behind the crack tip [43] Within this model for fracture of SMAs, dimensional analysis and manipulation of the constitutive law dictate that the normalized stresses, $\sigma_{ij}/\sigma_\infty$, strains, ε_{ij}/H_{sat}, and temperature, $C_M(T-M_s)/\sigma_\infty$ will be dependent on the following dimensionless parameters

$$\frac{E_A H_{sat}}{\sigma_\infty},\ k\sigma_\infty,\ \frac{C_M(A_s-M_s)}{\sigma_\infty},\ \frac{C_M(A_f-A_s)}{\sigma_\infty},\ \frac{C_M(M_s-M_f)}{\sigma_\infty},\ \frac{C_M}{C_A},$$

$$\frac{E_M}{E_A},\ \nu_M, \frac{\nu_M}{\nu_A}, \tag{4.1.2}$$

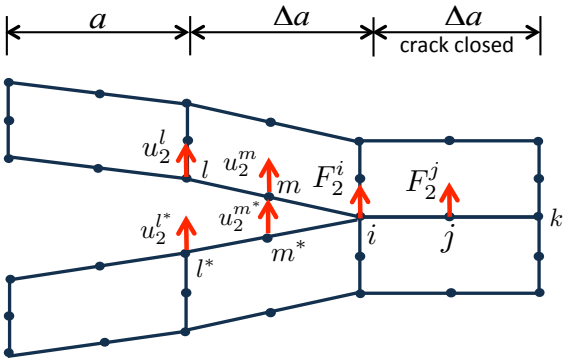

Figure 4.4: VCCT for eight-noded elements.

which are subject to the following inequalities

$$\frac{C_M(A_f - A_s)}{\sigma_\infty} \geq 0 \quad \text{and} \quad \frac{C_M(M_s - M_f)}{\sigma_\infty} \geq 0,$$

under the convention of tensile stresses being positive, since $M_f \leq M_s$, $A_s \leq A_f$. Note that, in what follows, the Poisson's ratios of the two phases are assumed approximately equal, *i.e.*, $\nu_A = \nu_M = \nu$, which is the case for most SMA material systems. Prior to presenting results on the driving force for crack growth and the mechanical fields close to the crack tip in SMAs during actuation, the influence of the non-dimensional parameters listed in Eq. (4.1.2) over the strain–temperature curve of a uniaxial isobaric test is presented. The numerical calculations are performed by considering the values of the parameters listed in (4.1.2) conformed to the material properties of typical NiTi systems (Table 4.1). $E_A H_{sat}/\sigma_\infty$ is the ratio of the ultimate transformation strain to the characteristic elastic strain in the material (Figure 4.5). If rearranged as $\sigma_\infty H_{sat}/\left[(\sigma_\infty)^2/E_A\right]$, it can also be interpreted as the ratio of "potential" energy due to transformation to elastic energy in the material. Similarly, $k\sigma_\infty$ is related to the maximum transformation strain attained for a given applied

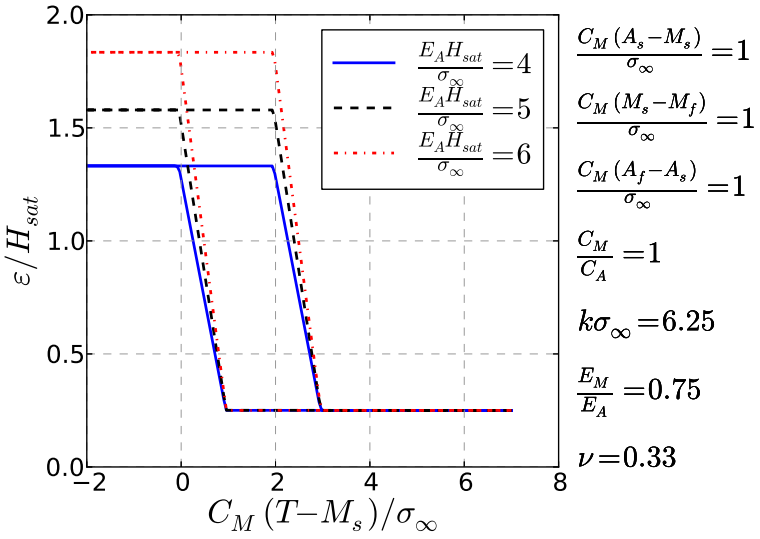

Figure 4.5: Strain–temperature response for a range of the non-dimensional parameter $E_A H_{sat}/\sigma_\infty$: $E_A H_{sat}/\sigma_\infty$ is related to the maximum attainable transformation strain

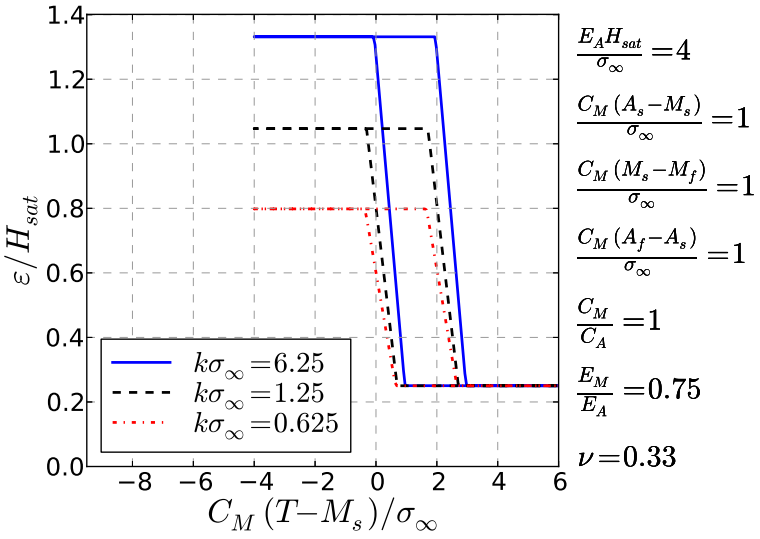

Figure 4.6: Strain–temperature response for a range of the non-dimensional parameter $k\sigma_\infty$: $k\sigma_\infty$ is related to the maximum transformation strain.

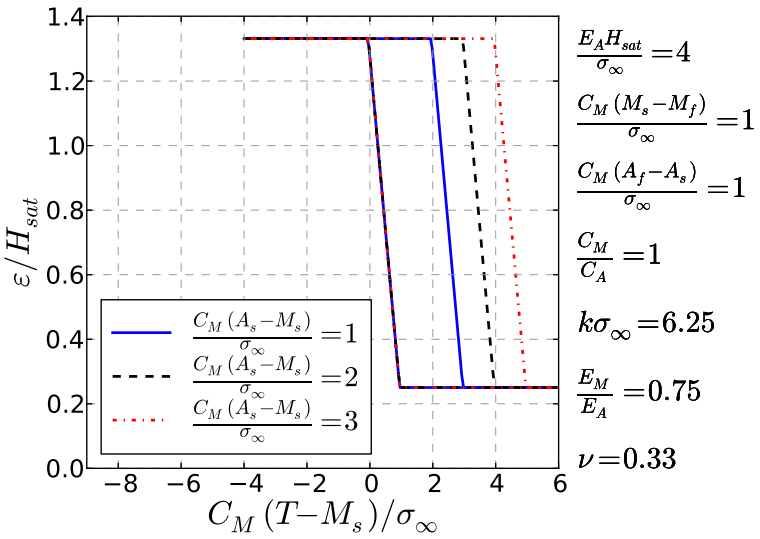

Figure 4.7: Strain–temperature response for a range of the non-dimensional parameter $C_M(A_s - M_s)/\sigma_\infty$: $C_M(A_s - M_s)/\sigma_\infty$ is related to the width of the hysteresis loop.

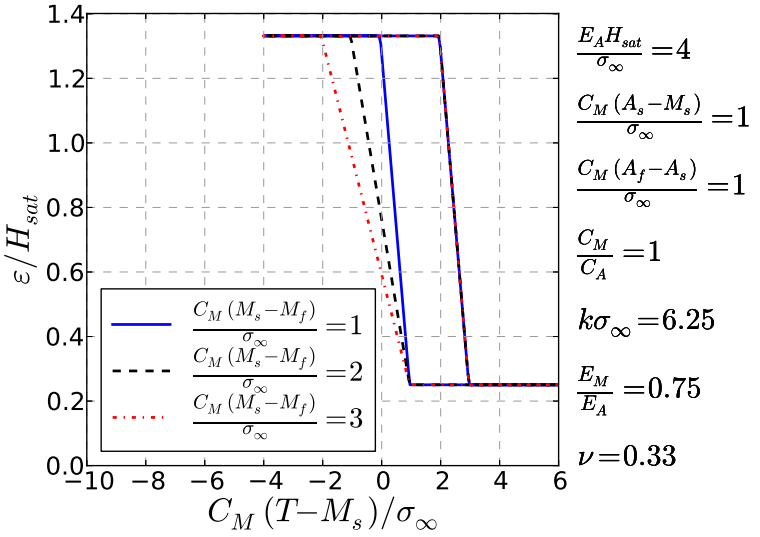

Figure 4.8: Strain–temperature response for a range of the non-dimensional parameter $(C_M)(M_s - M_f)/\sigma_\infty$: $(C_M)(M_s - M_f)/\sigma_\infty$ is related to the slope of the strain–temperature curve during forward transformation.

mechanical load (Figure 4.6). Higher values of $k\sigma_\infty$ result in higher transformation strains. The non-dimensional parameter $C_M(A_s - M_s)/\sigma_\infty$ is related to the area of the hysteresis loop (Figure 4.7), as it shifts the temperature range in which reverse phase transformation occurs during heating. The higher the value of $C_M(A_s - M_s)/\sigma_\infty$, the greater the area of the hysteresis loop. $C_M(M_s - M_f)/\sigma_\infty$ is related to the slope of the strain–temperature curve during forward phase transformation (transformation hardening) and $C_M(A_f - A_s)/\sigma_\infty$ to the slope of the strain–temperature curve during reverse phase transformation (Figure 4.8 and (Figure 4.9), respectively). Increasing values of $C_M(M_s - M_f)/\sigma_\infty$ and/or $C_M(A_f - A_s)/\sigma_\infty$ result in larger temperature ranges needed for forward and/or reverse phase transformation, respectively, to be completed once initiated. The influence of parameter C_M/C_A is similar to that of parameter $C_M(A_s - M_s)/\sigma_\infty$ (Figure 4.10) while the influence of the elastic properties of the two phases on the thermo-mechanical response is considered straightforward and is not commented here.

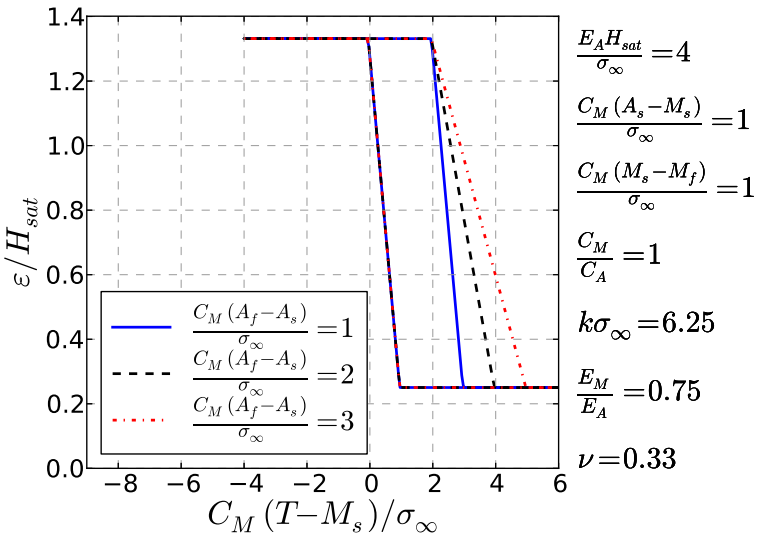

Figure 4.9: Strain–temperature response for a range of the non-dimensional parameter $C_M(A_f - A_s)/\sigma_\infty$: $C_M(A_f - A_s)/\sigma_\infty$ is related to the slope of the strain–temperature curve during reverse phase transformation.

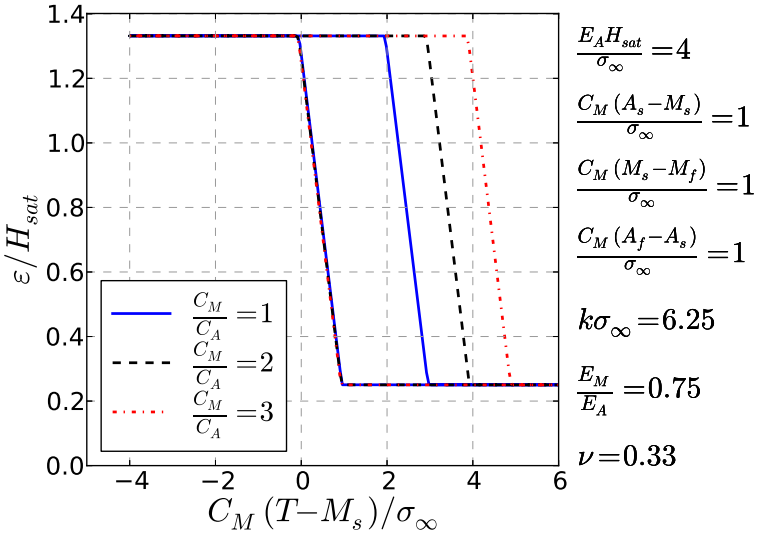

Figure 4.10: Strain–temperature response for a range of the non-dimensional parameter C_M/C_A: C_M/C_A has the same influence as that of parameter $C_M(A_s - M_s)/\sigma_\infty$ (Figure 4.10).

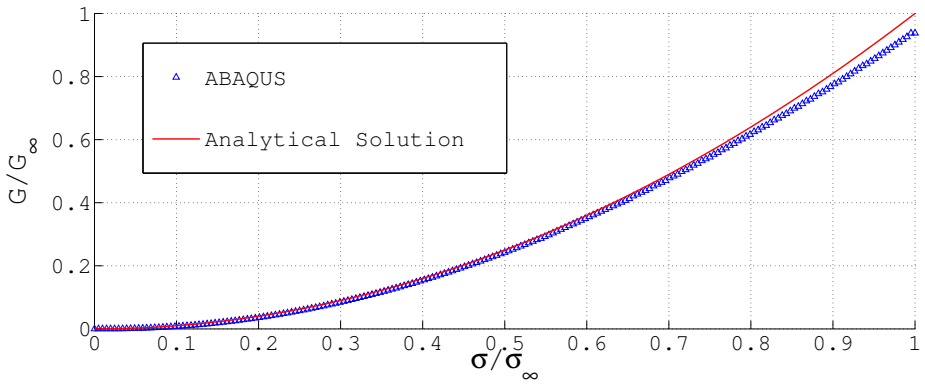

Figure 4.11: Comparison between the energy release rate, calculated at the end of mechanical loading under small scale transformation conditions, and the analytical solution for this geometry.

4.2 Crack Driving Force Predictions

The effect of global thermo-mechanically-induced phase transformation on the driving force for crack growth during actuation, as given by the ratio G_I/G_∞, is now examined, where G_∞ corresponds to the value of the energy release rate at $T = T_h$ before thermal cycling. Under plane strain conditions and assuming that any non-proportional loading effects near a stationary crack in these materials can be neglected, the path-independence of the J-integral implies that the energy release rate at $T = T_h$ is given by

$$G_\infty = \frac{1-\nu^2}{E_A} K_{\sigma_\infty}^2, \quad \text{where } K_{\sigma_\infty} = \sigma_\infty \sqrt{\pi a}. \tag{4.2.3}$$

The numerical calculations confirm, within a % 5 error, the above expression for G_∞ (Figure 4.11). This expression is valid due to the small scale transformation conditions assumed for the stress-induced phase transformation occurring close to the crack tip by applying a sufficiently low far-field stress, σ_∞, at a sufficiently

high temperature, T_h. Dimensional analysis dictates that the ratio G_I/G_∞ should be dependent upon the non-dimensional parameters listed in (4.1.2). As shown in Figure 4.12, during cooling, the energy release rate initially increases until it reaches a peak and then decreases before attaining a value at temperature $T = M_f$, at which the whole material is fully transformed, which remains constant under cooling at lower temperatures. During heating, the energy release rate starts increasing at temperature $T = A_s$, at which reverse phase transformation initiates, then, after reaching a peak, it decreases before attaining, eventually, a constant value. Note that *(i)* the energy release rate at the end of heating is the same with the energy release rate, G_∞, at the beginning of cooling, and *(ii)* the peak value of the energy release rate during heating is higher than the peak value during cooling. Numerical calculations show that the normalized ratio G_I/G_∞ is independent on the crack length $2a$, an expected result since the crack length is the only length scale of the considered fracture problem. Moreover, as it can be inferred from Figure 4.13, the strains due to thermal expansion do not affect the energy release rate. As a matter of fact, for most of the NiTi systems the coefficient of thermal expansion, α, which usually assumes the same value for both martensite and austenite, is of the order of 10^{-6}, therefore, in relation to the temperature variations adopted in the present study, their contribution can be neglected. An insight into above described results can be obtained from a basic analysis, to be presented below, carried out in [16, 48] for studying transformation toughening in ceramics containing particles that undergo stress-induced transformation. To this end, some features of the mechanical fields are now given. The stresses near the crack tip increase severely as expected, in fact, the numerical results suggest that close to the crack tip the stresses have a $1/\sqrt{r}$ radial asymptotic behavior during thermal cycling. In Figure 4.14, the angular dependence of the SMA stress field close to the crack tip at the end of cooling is compared to the

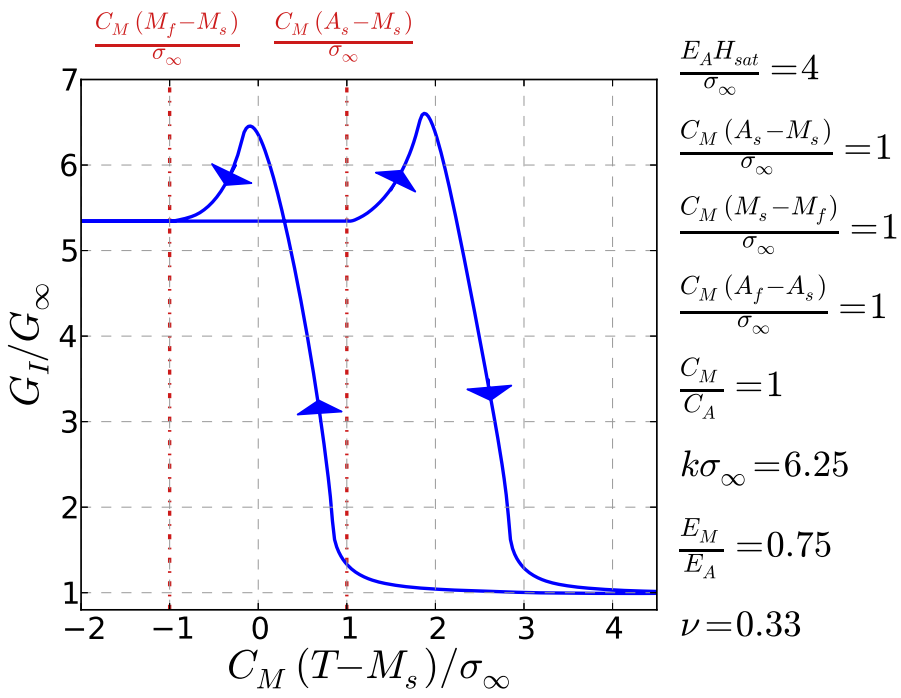

Figure 4.12: Normalized energy release rate, G_I/G_∞, versus normalized temperature, $C_M(T - M_s)/\sigma_\infty$.

angular dependence of the calculated stress field for an isotropic elastic solid with the elastic properties of martensite. The values of the non-dimensional parameters used in the calculations are those of Figure 4.12 and the energy release rate used in the normalization corresponds to the computed value at the end of cooling. According to the calculations, the stress fields are equivalent. This result holds true through out the thermal loading path and can be explained by the linear elastic response of the martensitic region that exists close to the crack tip. Therefore, the stress and strain fields close to the crack tip can be characterized by the stress intensity factor,

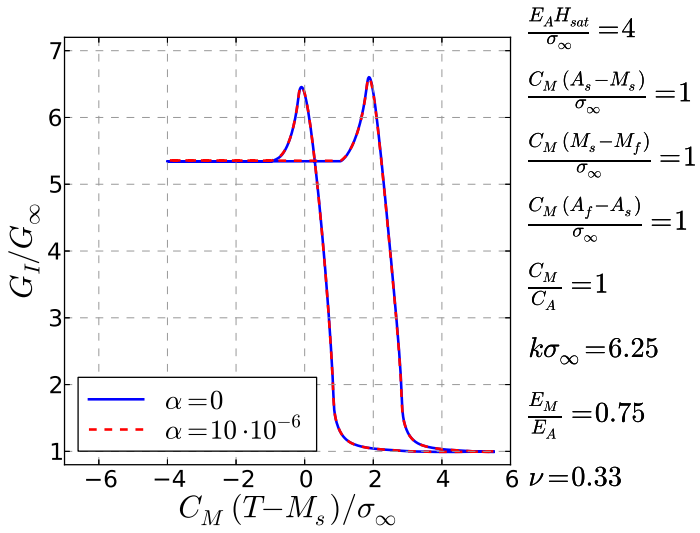

Figure 4.13: Effect of thermal expansion on the normalized energy release rate, G_I/G_∞, versus normalized temperature, $C_M(T - M_s)/\sigma_\infty$.

K_I, which is related to the energy release rate, G_I, under plane strain conditions by

$$G_I = \frac{1-\nu^2}{E_M} K_I^2. \tag{4.2.4}$$

Note that the crack-tip stress intensity factor K_∞ at $T = T_h$ is *not* equal to K_{σ_∞}, which is the far-field stress intensity factor at that temperature. The relationship between them reads as $K_\infty = K_{\sigma_\infty} E_M/E_A$.

In order to obtain an insight into the numerical results concerning the effect of actuation on the energy release rate G_I or equivalently on the stress intensity factor K_I in SMAs, K_I can be related to K_∞ through

$$K_I = K_\infty + \Delta K_I, \tag{4.2.5}$$

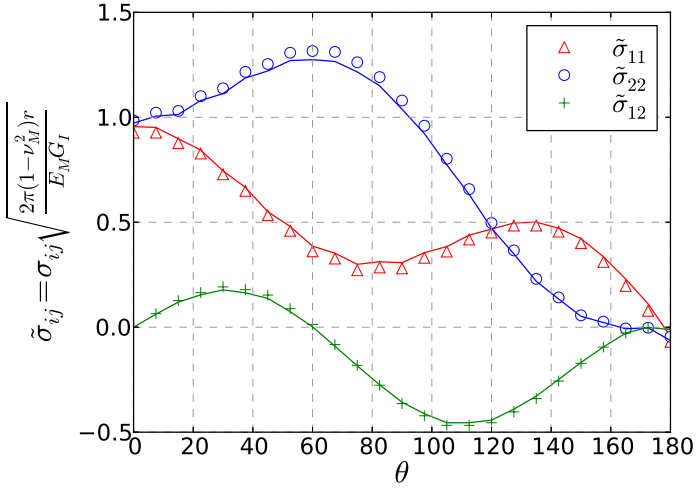

Figure 4.14: Angular distribution of stresses close to the crack tip at the end of cooling. The markers are the numerical results for the SMA material and the solid lines are numerical results for an elastic material with the properties of martensite. The $1/\sqrt{r}$ radial dependence has been accounted for within the normalization.

where

$$\Delta K_I = \iint_{\Omega} dK_I, \tag{4.2.6}$$

determines the enhancement/reduction in the stress intensity factor due to transformation. In the above equation (4.2.6), Ω is the upper half of the transformed region and dK_I is the enhancement/reduction in the stress intensity function due to two differential elements of area dA undergoing a transformation strain (Figure 4.15). These two are symmetrically located with respect to the plane of the crack so that mode I conditions prevail, the one at (r, β) with respect to the crack tip, characterized by the stress-free strains $\{\varepsilon_{11}^t,\ \varepsilon_{22}^t,\ \varepsilon_{12}^t\}$ for plane strain loading, and the other one at $(r, -\beta)$, characterized by $\{\varepsilon_{11}^t,\ \varepsilon_{22}^t,\ -\varepsilon_{12}^t\}$. For differential elements

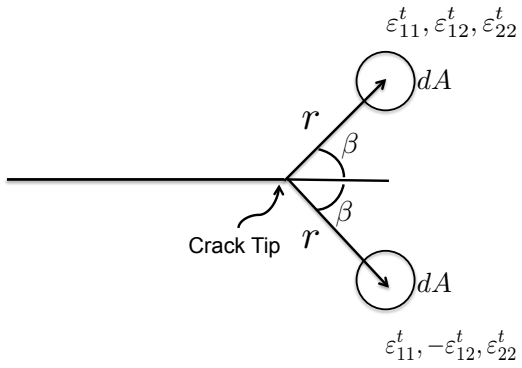

Figure 4.15: Material elements undergoing phase transformation symmetrically placed ahead of the crack tip.

close to the crack tip, an explicit form of dK_I can be obtained

$$dK_I = \frac{1}{\sqrt{8\pi}} \frac{E_M dA}{1-\nu_M^2} r^{-3/2} M\left(\varepsilon_{\gamma\delta}^t, \beta\right), \tag{4.2.7}$$

where

$$M\left(\varepsilon_{\gamma\delta}^t, \beta\right) = \varepsilon_{\alpha\alpha}^t \cos\frac{3\beta}{2} + 3\varepsilon_{12}^t \cos\frac{5\beta}{2}\sin\beta + \frac{3}{2}\left(\varepsilon_{22}^t - \varepsilon_{11}^t\right)\sin\frac{5\beta}{2}\sin\beta, \tag{4.2.8}$$

with the Greek indices ranging over 1 to 2 and the repeated Greek index indicating a sum over 1 and 2. From (4.2.7) and (4.2.8) it can be concluded that there is fan ahead of the crack tip, such that any transformed material which falls within this fan and at sufficiently small distances from the crack tip increases the near-tip intensity and consequently the energy release rate, while transformed material behind this fan reduces that intensity. For pure dilatational transformation, the fan is of 120^o, whereas for pure shear transformation strain, *i.e.*, $\varepsilon_{12}^t \neq 0$, $\varepsilon_{11}^t = \varepsilon_{22}^t = 0$, the corresponding fan is of 72^o. It can be noticed that when stress-free strains are generated by area elements transforming ahead of the crack tip (Figure 4.15),

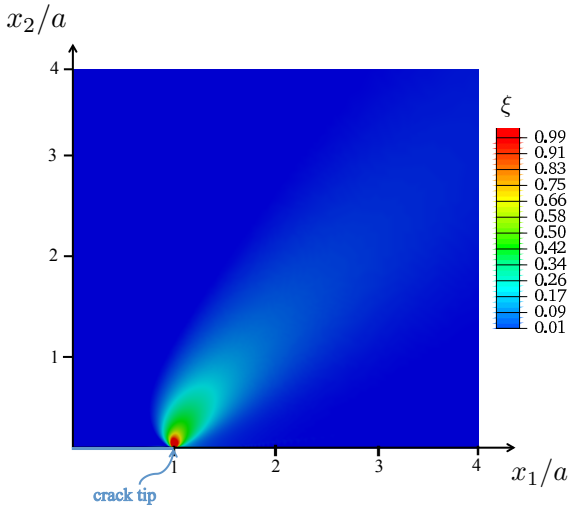

Figure 4.16: Martensite volume fraction, ξ, during cooling at the temperature greater than that at which G_I/G_∞ attains its maximum value.

the surrounding material undergoes a state of compressive stresses which induces the crack surfaces to open. Conversely, when material elements are transformed behind the crack tip closure stresses are placed by the rest of the material on the crack surfaces resulting in crack closure. On the basis of the above analysis, the following insight into the effect of thermal loading into the energy release rate for the specific center-cracked configuration investigated here can be obtained: the energy release rate initially increases during cooling since the material first transforms in front of the crack tip and the subsequent decrease once the peak is reached is due to transformation occurring in the region behind the crack tip (Figure 4.16 and Figure 4.17).

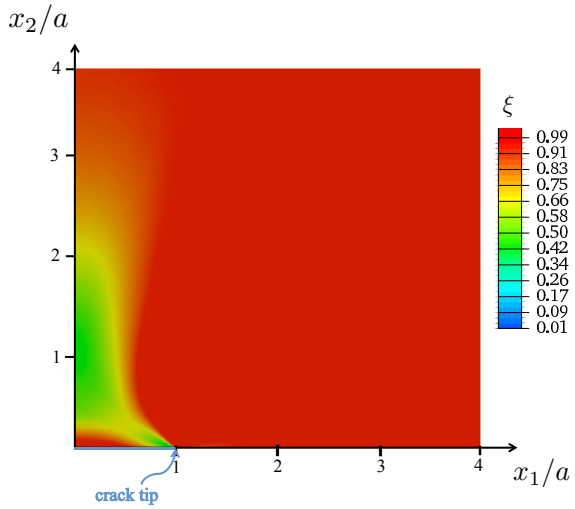

Figure 4.17: Martensite volume fraction, ξ, during cooling at the temperature at which G_I/G_∞ attains its maximum value.

4.3 Sensitivity of the Crack-Tip Energy Release Rate on Models Parameters

The sensitivity of the energy release rate during actuation on the key non-dimensional parameters given in (4.1.2) is examined next. The results to be presented can be rationalized on the basis of the analysis presented above and the effect of the non-dimensional parameters on the strain–temperature response under a uniaxial isobaric test. In Figure 4.18, it can be seen that through out the thermal cycling process the energy release rate increases monotonically as the relative ultimate transformation strain, $E_A H_{sat}/\sigma_\infty$, increases. Larger relative ultimate transformation strains imply higher stress-free strains which, in accordance to the analysis described above, implies a higher energy release rate. The effect of $k\sigma_\infty$ on the energy release rate is similar to that of $E_A H_{sat}/\sigma_\infty$, since $k\sigma_\infty$ is related to maximum transformation strain attained at a level of applied mechanical load, which is greater for higher values of

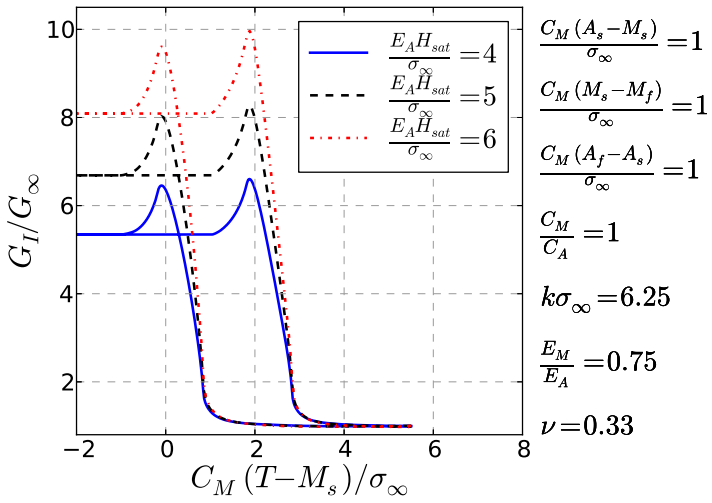

Figure 4.18: Normalized energy release rate, G_I/G_∞, versus normalized temperature, $C_M(T-M_s)/\sigma_\infty$, for a range of the non-dimensional parameter $E_A H_{sat}/\sigma_\infty$.

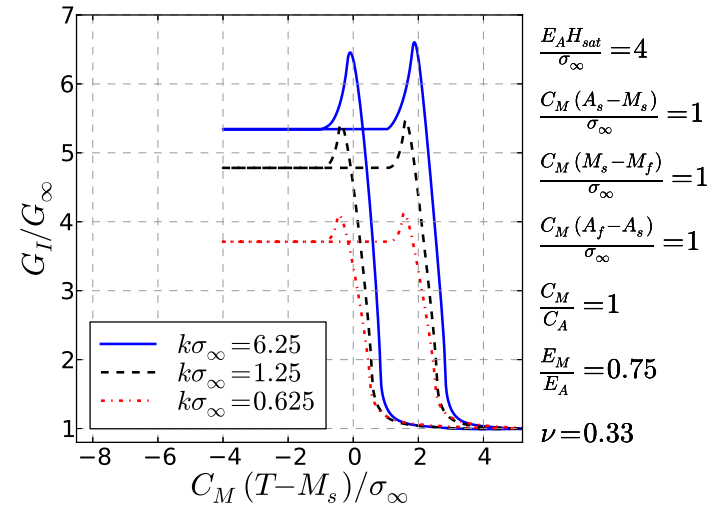

Figure 4.19: Normalized energy release rate, G_I/G_∞, versus normalized temperature, $C_M(T-M_s)/\sigma_\infty$, for a range of the non-dimensional parameter $k\sigma_\infty$.

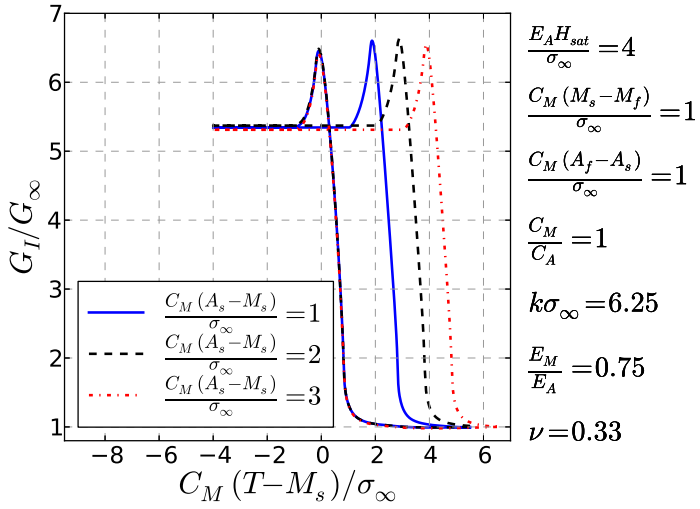

Figure 4.20: Normalized energy release rate, G_I/G_∞, versus normalized temperature, $C_M(T-M_s)/\sigma_\infty$, for a range of the non-dimensional parameter $C_M(A_s-M_s)/\sigma_\infty$.

$k\sigma_\infty$. The effect of $(A_s-M_s)/(T-M_s)$ on the energy release rate, presented in Figure 4.21, can be inferred directly from the influence of this parameter over the strain–temperature curve in a uniaxial isobaric test. Higher values of $(A_s-M_s)/(T-M_s)$ shift reverse phase transformation into a higher temperature range with an analogous effect on the energy release rate vs temperature response. The non-dimensional parameter $(M_s-M_f)/(T-M_s)$ has an impact on the slope of the energy release rate vs temperature curve during cooling, the constant value of energy release rate attained once the whole material is fully transformed from austenite to martensite, and the peak values attained during cooling and heating, all of them getting lower for higher values of $(M_s-M_f)/(T-M_s)$, *i.e.*, for increasing levels of transformation hardening. Higher values of $(A_f-A_s)/(T-M_s)$ result in lower slopes of the energy release rate vs temperature curve and peak values during heating (Figure 4.23). Increasing values of C_M/C_A result in higher peak values during heating (Figure 4.22). Finally, decreasing

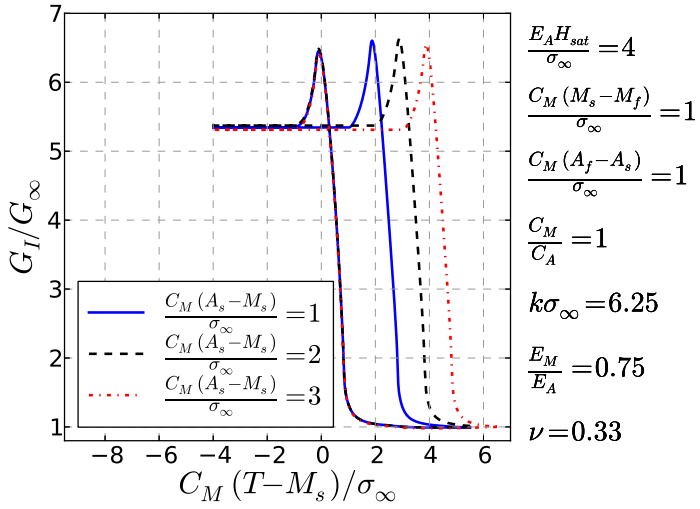

Figure 4.21: Normalized energy release rate, G_I/G_∞, versus normalized temperature, $C_M(T - M_s)/\sigma_\infty$, for a range of the non-dimensional parameter $C_M(A_s - M_s)/\sigma_\infty$.

values of E_M/E_A and/or increasing values of ν result in higher energy release rates through out the thermal cycling process. Since most of the non-dimensional parameters listed in Eq. 4.1.2 depend on the in-plane uniform uniaxial tensile stress at infinity σ_∞ and therefore are not material parameters, it is instructive to examine the influence of σ_∞ on the energy release rate (Figure 4.27). The numerical calculations in Figure 4.27 are for values of dimensional parameters chosen so as to conform with those of an SMA $Ni_{60}Ti_{40}$ (wt%) (Table 4.2) and yield quantitative results on the levels of energy release rate increase expected for this specific material during actuation. Also, as σ_∞ increases, the values of the non-dimensional parameters $E_A H_{sat}/\sigma_\infty$, $C_M(A_s - M_s)/\sigma_\infty$, $C_M(A_f - A_s)/\sigma_\infty$, $C_M(M_s - M_f/\sigma_\infty$, C_M/C_A decrease while the value of $k\sigma_\infty$ increases. The net outcome is a decrease of the ratio G_I/G_∞ for decreasing values of far-field stress σ_∞.

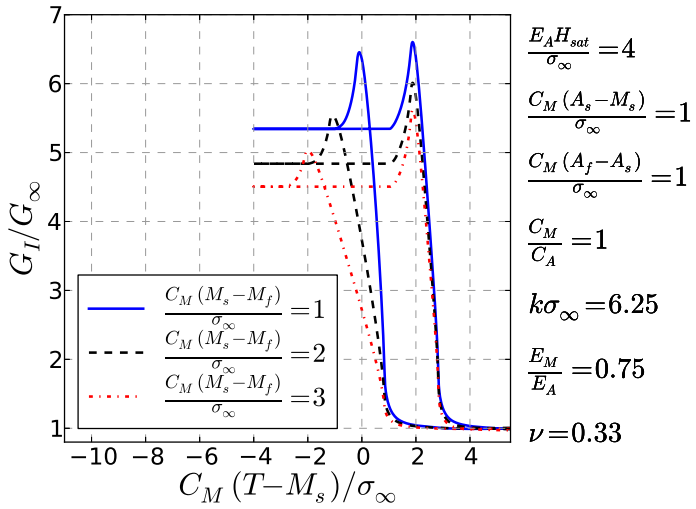

Figure 4.22: Normalized energy release rate, G_I/G_∞, versus normalized temperature, $C_M(T-M_s)/\sigma_\infty$, for a range of the non-dimensional parameter $C_M(M_s-M_f)/\sigma_\infty$.

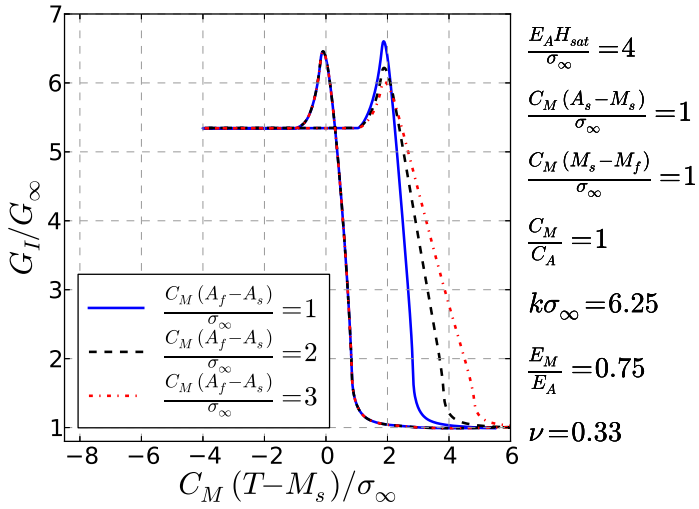

Figure 4.23: Normalized energy release rate, G_I/G_∞, versus normalized temperature, $C_M(T-M_s)/\sigma_\infty$, for a range of the non-dimensional parameter $C_M(A_f-A_s)/\sigma_\infty$.

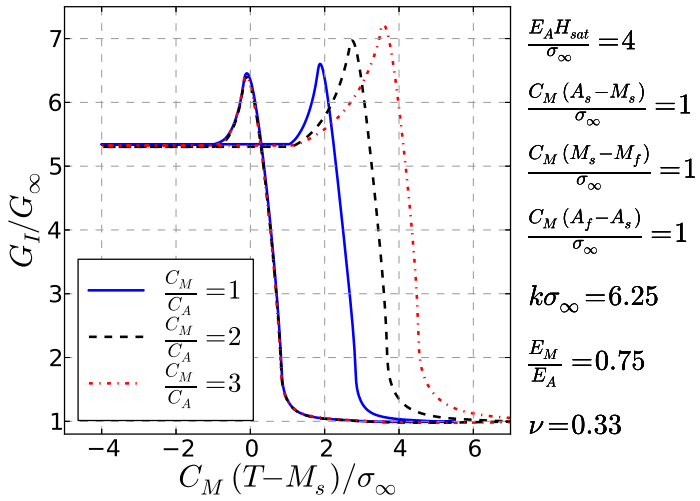

Figure 4.24: Normalized energy release rate, G_I/G_∞, versus normalized temperature, $C_M(T-M_s)/\sigma_\infty$, for a range of the non-dimensional parameter C_M/C_A.

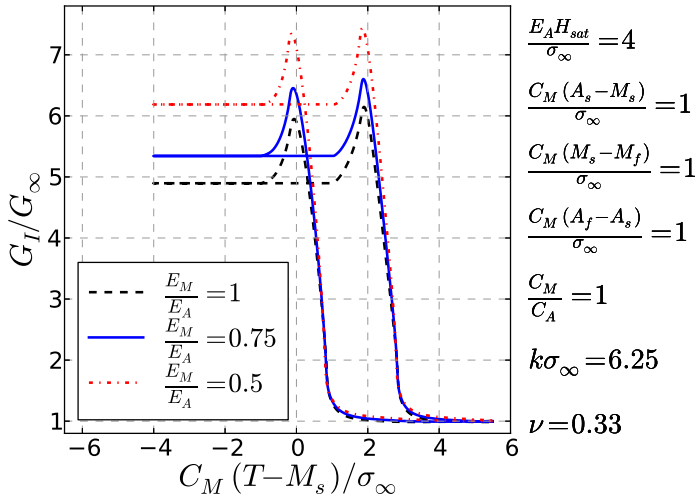

Figure 4.25: Normalized energy release rate, G_I/G_∞, versus normalized temperature, $C_M(T-M_s)/\sigma_\infty$, for a range of the non-dimensional parameter E_M/E_A.

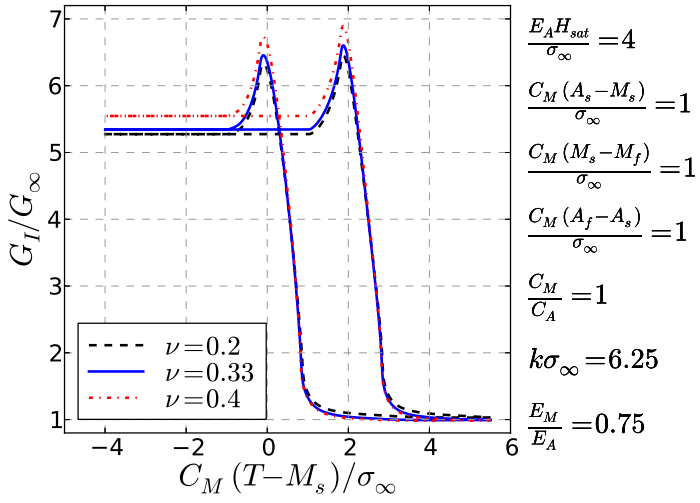

Figure 4.26: Normalized energy release rate, G_I/G_∞, versus normalized temperature, $C_M(T - M_s)/\sigma_\infty$, for a range of Poisson ratio ν.

Table 4.2: Parameter values used for the numerical results presented in Figure 4.27. These values correspond to $Ni_{60}Ti_{40}$ (wt%)

parameter	value	parameter	value
E_A (MPa)	75150	H_{sat}	0.0119
E_M (MPa)	51000	k (MPa^{-1})	0.0022
$\nu_A = \nu_M$	0.33	M_f (^{o}K)	268
A_s (^{o}K)	293	M_s (^{o}K)	357
A_f (^{o}K)	372	C_M (MPa $^o\text{K}^{-1}$)	23.55
C_A (MPa $^o\text{K}^{-1}$)	22.16		

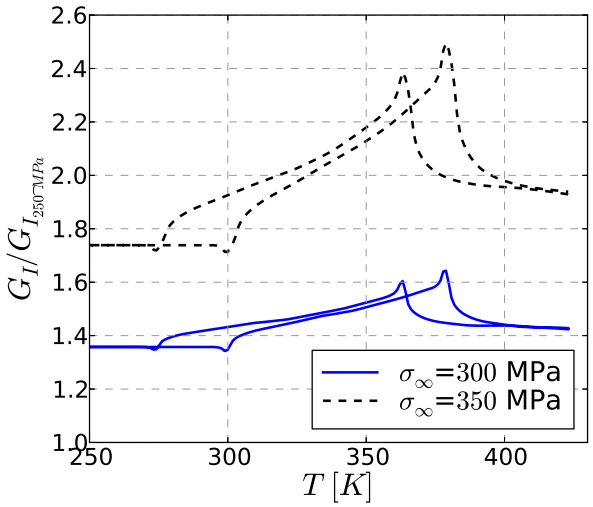

Figure 4.27: Normalized energy release rate, G_I/G_∞, versus temperature T, for values of the non-dimensional parameters chosen so as to conform with those of $Ni_{60}Ti_{40}$ (wt%) (Table 4.2)

5. CONCLUSIONS AND FUTURE WORK*

In this thesis, finite element calculations have been performed to study the effect of phase transformation on the fracture behavior of SMAs in order to provide some guidelines for their effective use in several industrial and biomedical applications. Some of the future works which could further improve the developments of such an understanding are outlined.

5.1 Summary of the Key Findings

In Chapter 3, the effect of stress-induced phase transformation on the fracture behavior of pseudoelastic SMAs, initially in austenitic state, subjected to nominally isothermal, mode I, plane strain loading conditions, has been investigated. The constitutive response of the material has been taken to be characteristic of polycrystalline SMAs with the constitutive law accounting for the generation and recovery of all martensitic variants in a volume average sense. Small scale transformation conditions have been assumed according to which the actual boundary conditions have been replaced by the linear-elastic inverse-square-root strain distribution far away from the crack tip. It has been found that:

- The crack tip mechanical fields around a *stationary* crack recover the asymptotic behavior of an elastic isotropic material and therefore can be uniquely described by only one parameter, namely the energy release rate G_I. Moreover, numerical calculations performed by Baxevanis et al. [8] showed that, when the constitutive law is extended to account for plastic deformation, the

*Part of this chapter is reprinted with permission from "On the fracture toughness enhancement due to stress-induced phase transformation in shape memory alloys" by Baxevanis, T., Parrinello, A.F., Lagoudas, D.C., 2013, International Journal of Plasticity. doi: http://dx.doi.org/10.1016/j.ijplas.2013.04.007

size of the resulting plastic zone around the crack tip is an order of magnitude smaller than that expected in conventional elastic-plastic material. Based on these findings, and on experimental evidence that at least NiTi systems with partially decoherent precipitates are characterized by cleavage-like fracture, a fracture point criterion has been postulated. In particular, the size of the fracture process zone has been assumed to be small compared to all the characteristic length scales involved in the problem, thus a constitutive law which does not account for plastic deformation has been employed. Therefore, the quasi-static stable crack growth has been modeled by assuming that the crack tip proceeds at a critical level of the energy release rate.

- The computations have shown increased fracture toughness associated with closure stresses placed on the crack tip by the transformed material left behind in the wake of the advancing crack tip. For the temperature range assumed, the dependence of transformation toughening on the maximum transformation strain, transformation hardening, mismatch of the Youngs moduli of the two phases, and temperature is relatively strong implying that the actual shape of the uniaxial isothermal stress–strain curve for stress levels below plastic yielding is important for the quantitative determination of the transformation toughening.

- The constitutive law has been extended in order to investigate the effect of plastic deformation on the fracture toughness of superelastic shape memory alloys and a cohesive zone model has been employed to model the fracture process zone. However, the contribution of plastic deformation can only be determined through a careful comparison between simulation and experimental data on crack growth. Nonetheless, the aforementioned evidences have indicated that

plastic dissipation during crack growth might be only a small fraction of the energy dissipated due to phase transformation.

In Chapter 4, finite element calculations have been carried out to investigate the effect of global thermo-mechanically-induced phase transformation on the mechanical fields close to the crack tip and the driving force for crack growth in SMAs. The study has focused on the prototype problem of an infinite center-cracked austenitic SMA plate subjected to a thermal actuation cycle under isobaric, plane strain, mode I conditions. The constitutive response of the material has been taken to be the same as that adopted in the previous chapter. According to the calculations it has been found that:

- An elastically deformed martensite zone exists close to the crack tip through out the loading path, in which the stress and strain fields close to the crack tip recover the asymptotic behavior of an isotropic elastic material. The VCCT has been employed to calculate the change in the crack-tip energy release rate. During cooling, the energy release rate initially increases as a result of martensitic transformation until it reaches a peak and then decreases before attaining a value at the martensitic-finish temperature, M_f which remains constant under further cooling. During heating, the crack-tip energy release rate starts increasing at the austenitic-start temperature, A_s, at which reverse phase transformation initiates, then, after reaching a peak, it decreases before attaining, eventually, a constant value. The peak value of the crack-tip energy release rate during heating has been found to be higher than the corresponding peak during cooling.

- The increase of the crack-tip energy release rate during thermal actuation is substantial, an order of magnitude for some material systems. If crack growth

is assumed to occur when the crack-tip energy release rate reaches a material specific critical value, then crack growth may occur during actuation as a result of phase transformation.

- The crack-tip energy release rate is strongly sensitive to the variation of key non-dimensional parameters characterizing the thermo-mechanically-induced phase transformation. In particular, the dependence of crack-tip energy release rate on the bias load, transformation strain, slopes of the strain–temperature curve during transformation, mismatch of Young's moduli between the two phases, and Poisson's ratio has pointed out that the actual shape of the isobaric strain–temperature curve is important for the quantitative determination of the expected increase in the crack-tip energy release rate during actuation.

5.2 Future Work

In this section, the future challenges that the author considers that should be addressed are outlined. The suggested future work concerns aspects of the fracture behavior of SMAs that expand the research framework that has been proposed in this thesis.

- Crack growth during thermal isobaric actuation should be investigated as a continuation of the studies presented in Chapter 4 with the critical crack-tip energy release assumed as a fracture criterion. The computations should be carried out on different geometry configurations since phase transformation is globally thermo-mechanically-induced implying that small scale transformation conditions do not apply and the solution is configuration-dependent. It is aimed to compare the obtained numerical computations against experiments in order to provide quantitative evaluations to be used in an effective design of SMA actuators. These findings can be used to develop a fracture based

understanding of the fatigue behavior under thermal cyclic isobaric loading conditions.

- Research should be performed in order to study the effect of phase transformation on the fracture behavior of SMAs subjected to dynamic loading conditions. As far as the pseudoelastic response is concerned, different strain rates should be considered and therefore the fully-coupled thermomechanical problem should be solved. The constitutive model adopted in this work has to be extended in order to account for the dissipation due to generation of latent heat. Moreover, the fracture characteristics of SMAs undergoing isobaric thermal actuation under different rates of temperature variations should be investigated. Thus, convection between the material and the surrounding and conduction through the medium should be included in the boundary value problem.

- Chapter III can be expanded in order to study the effect of stress-induced phase transformation on the fracture toughness enhancement during crack propagation under large scale transformation conditions. A modified boundary layer approach can be employed in order to take into account constraints due to geometry e loading conditions.

- The fracture behavior of textured polycrystalline SMAs should be investigated. In particular, the material should be considered to consist of a discrete texture of grains with different sizes and orientations. Thus, a constitutive model which accounts for the anisotropic behavior of the material should be employed. Crack propagation can be studied by means of meshless numerical techniques (*i.e.,* the extended finite element method) which are able to predict the evolution of the crack path during the analysis. The fracture criterion for the intragranular crack growth should be based on the critical energy release

rate, as each grain is supposed to behave as single crystal material which fails along preferential crystalline plane by cleavage. While a traction separation law should be employed to characterize the response of the interface between the grains and their progressive separation as crack growths.

REFERENCES

[1] Abaqus. *Analysis User's Manual*. Dassault Systèmes of America Corp., Woodlands Hills, CA, 2009.

[2] T.L Anderson. *Fracture mechanics: fundamentals and applications*, chapter 2. Taylor and Francis, Boca Ration,FL, 2005.

[3] J. Arghavani, F. Auricchio, R. Naghdabadi, A. Reali, and S. Sohrabpour. A 3-d phenomenological constitutive model for shape memory alloys under multiaxial loadings. *Int. J. Plast.*, 26:976–991, 2010.

[4] Raniecki B. and Lexcellent C. Thermodynamics of isotropic pseudo elasticity in shape memory alloys. *Eur. J Mech. A-Solid*, 17(2):1339–1368, 1998.

[5] L. Banks-Sills and Y. Bortman. Reappraisal of the quarter-point quadrilateral element in linear elastic fracture mechanics. *Int. J. Fract.*, 25:169–180, 1984.

[6] G.I Barenblatt. The formation of equilibrium cracks during brittle fracture. general ides and hypothesis. axially-simmetric cracks. *Prikl. Matem. I mekham*, 23:434–444, 1959.

[7] R.S. Barsoum. Application of quadratic isoparametric finite element in fracture mechanics. *Int. J. Numer. Meth Engng*, 10(25):603–605, 1976.

[8] T. Baxevanis, Y. Chemisky, and D. Lagoudas. Finite element analysis of the plane-strain crack-tip mechanical fields in pseudoelastic shape memory alloys. *Smart Mater. Struct.*, 21(9), 2012.

[9] T. Baxevanis and D. Lagoudas. A mode I fracture analysis of a center-cracked infinite shape memory alloy plate under plane stress. *Int. J. Fract.*, 175(2):151–166, 2012.

[10] T. Baxevanis, C.M. Landis, and D.C. Lagoudas. On the fracture toughness of pseudoelastic shape memory alloys. *Submitted*, 2013.

[11] V. Birman. On mode I fracture of shape memory alloy plates. *Smart Mater. Struct.*, 7:433–437, 1998.

[12] C. Bouvet, S. Calloch, and C. Lexcellent. A phenomenological model for pseudoelasticity of shape memory alloys under multiaxial proportional and nonproportional loadings. *Eur. J Mech. A-Solid*, 23(1):976–991, 2004.

[13] J. Boyd and D.C. Lagoudas. A thermodynamical constitutive model for shape memory materials. Part I: The monolithic shape memory alloy. *Int. J. Plast.*, 12:805–842, 1996.

[14] J. G. Boyd and D. C. Lagoudas. A thermodynamical constitutive model for shape memory materials. part ii. the sma composite material. *Int. J. Plast.*, 12(7):843 – 873, 1996.

[15] J.G. Boyd and D.C. Lagoudas. A thermodynamical constitutive model for shape memory materials. part i. the monolithic shape memory alloy. *Int. J. Plast.*, 12(6):805 – 842, 1996.

[16] B. Budniansky, J.W. Hutchinson, and J.C. Lambropoulos. Continuum theory of dilatant transformation toughening in ceramics. *Int. J. Solids Struct.*, 19:337–355, 1983.

[17] A. Bulbich. Nucleation on the crack tip and transformation toughness in crystals undergoing structural phase transitions. *J. Mater. Sci.*, 27(4):1070–1080, 1992.

[18] G.T. Camacho and M. Ortiz. Computational modeling of impact damage in brittle materials. *Int. J. Solids Struct.*, 33:2899–2938, 1996.

[19] D. Carka and C.M. Landis. The analysis of crack tip fields in ferroelastic materials. *Smart Mater. Struct.*, 20, 2011.

[20] B.D. Coleman and M.E. Gurtin. Thermodynamics with internal state variables. *J. Chem. Phys.*, 47(2):597–613, 1967.

[21] A. Creuziger, L.J. Bartol, K. Gall, and W.C. Crone. Fracture in single crystal NiTi. *J. Mech. Phys. Solids*, 56:2896–2905, 2008.

[22] S. Daly, A. Miller, G. Ravichandar, and K. Bhattacharya. An experimental investigation of crack initiation in thin sheets of nitinol. *Acta Mater.*, 55:6322–6330, 2007.

[23] Lagoudas D.C and Bhattacharya A. On the correspondence between micromechanical models for isothermal pseudoelastic response of shape memory alloys and preisach model for hysteresis. *Math. Mech. Solids*, 2(4):405–440, 1997.

[24] R. de Borst, M.A. Gutierrez, G.N. Wells, J.C. Remmers, and H. Askes. Cohesive-zone models, higher-order continuum theories and reliability methods for computational failure analysis. *Int. J. Numer. Meth. Engng.*, 60:289–315, 2004.

[25] Z.Z. Du and J.W. Hancock. The effect of non-singular stresses on crack-tip constraints. *J. Mech. Phys. Solids*, 39:555–567, 1991.

[26] D.S. Dugdale. Yielding of steel sheets containing slits. *J. Mech. Phys. Solids*, 8:100–104, 1960.

[27] Falk F. Pseudoelastic stressstrain curves of polycrystal- line shape memory alloys calculated from single crystal data. *Int. J. Eng. Sci.*, 27(3):277–284, 1990.

[28] S. A. Fawaz. Application of the virtual crack closure technique to calculate stress intensity factors for through carcks with an elliptical crack front. *Eng. Fract. Mech.*, 59(3):327–342, 1998.

[29] Y. Freed and L. Banks-Sills. Crack growth resistance of shape memory alloys by means of a cohesive zone mode. *J. Mech. Phys. Solids*, 55:2157–2180, 2007.

[30] K. Gall, N. Yang, H. Sehitoglu, and Y.I. Chumlyakov. Fracture of precipitated niti shape memory alloys. *Int. J. Fract.*, 109:189–207, 1998.

[31] X. Gao and L.C. Brinson. A simplified multivariant sma model based on invariant plane nature of martensitic transformation. *J. Intell. Mater. Syst. Struct.*, 13(12):795–810, 2002.

[32] P.H. Geubelle and J.S. Baylor. Impact-induced delamination of composites: a 2d simulation. *Comp. Part B-Eng.*, 29(B):589–602, 1988.

[33] S. Gollerthan, M.L. Young, A. Baruj, J. Frenzel, W.W. Schmahl, and G. Eggeler. Fracture mechanics and microstructure in NiTi shape memory alloys. *Acta Mater.*, 57:1015–1025, 2009.

[34] Liebowitz H. and Moyer E.T. Finite element methods in fracture mechanics. *Comput Struct*, 31:1–9, 1989.

[35] D. Hartl, D. Lagoudas, J. Mabe, F. Calkins, and J. Mooney. Use of Ni60Ti shape memory alloy for active jet engine chevron application, Part II: Experimentally validated numerical analysis. *Smart Mater. Struct.*, 19(1), 2009.

[36] D. J. Hartl and D. C. Lagoudas. Aerospace applications of shape memory alloys. Proceedings of the Institution of Mechanical Engineers, Part G: Journal of Aerospace Engineering, pages 535–552. SAGE, 2007.

[37] D.J. Hartl and D.C. Lagoudas. Constitutive modeling and structural analysis considering simultaneous phase transformation and plastic yield in shape memory alloys. *Smart Mater. Struct.*, 2009.

[38] R.D. Henshell and K.G. Shaw. Crack tip finite elements are unnecessary. *Int. J. Numer. Meth. Engng.*, 9(3):495–507, 1975.

[39] J.W. Hutchinson. Singular behavior at the end of a tensile crack in a hardening material. *J. Mech. Phys. Solids*, 16:13–31, 1968.

[40] G.R. Irwin. Analysis of stresses and strain near the of a crack traversing a plate. *J. Appl. Mech.*, 24:361–364, 1957.

[41] G.R. Irwin. *Handbuch der Physik VI*, chapter Fracture I, pages 558–590. Spinger Verlag, Berlin, Germany, 1958.

[42] S. Kobayashi K. Tanaka and Y. Sato. Thermomechanics of transformation pseudo elasticity and shape memory effect in alloys. *Int. J. Plast.*, 2:59–72, 1986.

[43] R. Krueger. Virtual crack closure technique: History, approach, and applications. *Appl. Mech. Rev.*, 57(2), 2004.

[44] D. C. Lagoudas, D. Hartl, Y. Chemisky, L. Machado, and P. Popov. Constitutive model for the numerical analysis of phase transformation in polycrystalline shape memory alloys. *Int. J. of Plast.*, 32-33:155–183, 2012.

[45] D.C. Lagoudas, editor. *Shape Memory Alloys: Modelling and Enginnering Applications*, pages 1–51. Springer, New-York, 2008.

[46] D.C. Lagoudas, editor. *Shape Memory Alloys: Modelling and Enginnering Applications*. Springer, New-York, 2008.

[47] D.C. Lagoudas, P.B. Entchev, P. Popov, E. Patoor, L.C. Brinson, and X. Gao. Shape memory alloys. Part II: Modeling of polycrystals. *Mech. Mater.*, 38:430–462, 2006.

[48] J.C. Lambropoulos. Shear, shape and orientation effects in transformation toughening. *Int. J. Solids Struct.*, 22:1083–1106, 1986.

[49] C. M. Landis. On the fracture toughness of ferroelastic materials. *J. Mech. Phys. Solids*, 51:1347–1369, 2003.

[50] S. Leclercq and C. Lexcellent. A general macroscopic description of the thermomechanical behavior of shape memory alloys. *J. Mech. Phys. Solids*, 44(6):953–980, 1996.

[51] C. Lexcellent, M. R. Laydi, and V. Taillebot. Analytical prediction of the phase transformation onset zone at a crack tip of a shape memory alloy exhibiting asymmetry between tension and compression. *Int. J. Fract.*, 169(1):1–13, 2011.

[52] C. Lexcellent, R. M. Laydi, and V. Taillebot. Impact of the choice of a 3D thermomechanical model for shape memory alloys on the fracture and the delamination predictions. In *Procedia Engineering*, volume 10, pages 2232–2237, 2011.

[53] C. Lexcellent and F. Thiebaud. Determination of the phase transformation zone at a crack tip in a shape memory alloy exhibiting assymetry between tension and compression. *Scripta Mater.*, 59:321–323, 2008.

[54] H. Li and N. Chandra. Analysis of crack growth and crack-tip plasticity in ductile materials using cohesive zone models. *Int. J. Plast.*, 19:849–882, 2003.

[55] C. Liang and C. A. Rogers. One-dimensional thermomechanical constitutive relations for shape memory materials. *J. Intell. Mater. Syst. Struct.*, 1:207–234,

1990.

[56] C. Maletta and F. Furgiuele. Analytical modeling of stress-induced martensitic transformation in the crack tip region of nickel-titanium alloys. *Acta Mater.*, 58:92–101, 2010.

[57] C. Maletta and F. Furgiuele. Fracture control parameters for NiTi based shape memory alloys. *Int. J. Solids Struct.*, 48:1658–1664, 2011.

[58] R.M. McMeeking and A.G. Evans. Mechanics of transformation-toughening in brittle materials. *J. Am. Ceram. Soc.*, 65:242–246, 1982.

[59] F. Migliavacca, L. Petrini, M. Colombo, F. Auricchio, and R. Pietrabissa. Mechanical behavior of coronary stents investigated through the finite element method. *J. Biomech.*, 35:803–811, 2002.

[60] A. Needleman. An analysis of tensile decohesion along an interface. *J. Mech. Phys. Solids*, 38(3):289–324, 1990.

[61] A. Nespoli, S. Besseghini, S. Pittaccio, E. Villa, and S. Viscuso. The high potential of shape memory alloys in developing miniature mechanical devices: A review on shape memory alloy mini-actuators. *Sensors Actuat. A-Phys.l*, 158(1):149–160, 2010.

[62] M. Ortiz and A. Pandofli. Finite-deformation irreversible cohesive elements for three- dimensional crack-propagation analysis. *Int. J. Numer. Meth. Engng.*, 44:1267–1282, 1999.

[63] V.P. Panoskaltsis, S. Bahuguna, and D. Soldatos. On the thermomechanical modeling of shape memory alloys. *Int. J. Non-Linear Mech.*, 39:709–722, 2004.

[64] E. Patoor, D.C. Lagoudas, P.B. Entchev, L.C. Brinson, and X. Gao. Shape memory alloys. Part I: General properties and modeling of single crystals. *Mech. Mater.*, 38:391–429, 2006.

[65] Eberhard A. Patoor E. and M. Berveiller. Potentiel pseudoe' lastique et plasticite de transformation martensitique dans les mono et polycristaux me' talliques. *Acta Metall.*, 35:27792789., 1987.

[66] P. Popov and D. C. Lagoudas. A 3-D constitutive model for shape memory alloys incorporating pseudoelasticity and detwinning of self-accommodated martensite. *Int. J. Plast.*, 23(10 – 11):1679 – 1720, 2007.

[67] M.A. Qidwai and D.C. Lagoudas. On the thermodynamics and transformation surfaces of polycrystalline niti shape memory alloy material. *Int. J. Plast.*, 16:1309–1343, 2000.

[68] M.A. Qidwai and D.C. Lagoudas. Numerical implementation of a shape memory alloy thermomechanical constitutive model using return mapping algorithm. *Int. J. Plast.*, 16:1123–1168, 2000a.

[69] J. Rice. Limitation to the small scale yielding approximation for crack tip plasticity. *J. Mech. Phys. Solids*, 22:17–26, 1974.

[70] J. R. Rice, W. J. Drugan, and T. L. Sham. Elastic-plastic analysis of growing cracks. In *ASTM Special Technical Publication*, pages 189–221, 1980.

[71] J.R. Rice. A path independent integral and approximate analysis of strain concentration by notches and cracks. *J. Appl. Mech-T ASME.*, 35:379–386, 1968.

[72] J.R. Rice and G.F. Rosengren. Plane strain deformation near a crack tip in a power-law hardening material. *J. Mech. Phys. Solids*, 16:1–12, 1968.

[73] S. Robertson and R. Ritchie. In vitro fatigue-crack growth and fracture toughness behavior of thin-walled superelastic nitinol tube for endovascular stents: A basis for defining the effect of crack-like defects. *Biomat*, 28:700–709, 2007.

[74] S.W. Robertson, A. Metha, A.R. Pelton, and R.O. Ritchie. Evolution of crack-tip transformation zones in superelastic Nitinol subjected to in situ fatigue: A fracture mechanics and synchrotron X-ray micro-diffraction analysis. *Acta Mater.*, 55:6198–6207, 2007.

[75] E. Rybicki and M. Kanninen. A finite element calculation of stress intensity factors by a modified crack closure integral. *Eng. Fract. Mech.*, 9:931–938, 1977.

[76] K.N. Shivakumar, P.W. Tan, and J.C. Newman. A virtual crack-closure technique for calculating stress intensity factors for cracked three dimensional bodies. *Int. J. Fract.*, 36:43–50, 1988.

[77] N. Siegmund, T. Fleck and A. Needleman. Dynamic crack growth across an interface. *Int. J. Fract.*, 85:381–402, 1997.

[78] T. Siegmund and A. Needleman. A numerical study on dynamic crack growth in elastic-viscoplastic. *Int. J. Solids Struct.*, 43:769–787, 1997.

[79] J.C. Simo and T.J.R. Hughes. *Computational Inelasticity*, volume 7 of Interdisciplinary Applied Mathematics. Springer-Verlag, New York, 1998.

[80] G. Song, N. Ma, and H-N Li. Application of shape memory alloys in civil structures. *Eng. Struct.*, 28:1266–1274, 2006.

[81] M. Sreekumar, T. Nagarajan, M. Singaperumal, M. Zoppi, and R. Molfino. Critical review of current trends in shape memory alloy actuators for intelligent robots. *Indust. Robot*, 34(4):285–294, 2007.

[82] G. Stam and E. van der Giessen. Effect of reversible phase transformations on crack growth. *Mech. Mater.*, 21:51–71, 1995.

[83] D. M. Stump and B. Budiansky. Crack-growth resistance in transformation-toughened ceramics. *Int. J. Solids Struct.*, 25(6):635–646, 1989.

[84] Q. Sun, K. Hwang, and S. Yu. A micromechanics constitutive model of transformation plasticity with shear and dilatation effect. *J. Mech. Phys. Solids*, 39:507524, 1991.

[85] Q.P. Sun and K..C. Hwang. Micromechanics modelling for the constitutive behavior of polycrystalline shape memory alloy – II. study of the individual phenomena. *J. Mech. Phys. Solids*, 41:19–33, 1993.

[86] Q.P. Sun and K.C. Hwang. Micromechanics modelling for the constitutive behavior of polycrystalline shape memory alloys – I. derivation of general relations. *J. Mech. Phys. Solids*, 41:1–17, 1993.

[87] V. Taillebot, C. Lexcellent, and P. Vacher. About the transformation phase zones of shape memory alloys' fracture tests on single edge-cracked specimen. *Func. Mater. Lett.*, 5(1), 2012.

[88] K. Tanaka. A thermomechanical sketch of shape memory effect: One-dimensional tensile behavior. *Res. Mech.*, 18:251–263, 1986.

[89] A. Turon, P.P. Davila, C.G. Camanho, and J. Costa. An engineering solution for mesh size effects in the simulation of delamination using cohesive zone models. *Eng. Fract. Mech.*, 74:1665–1682, 2007.

[90] V. Tvergaad and J. W. Hutchinson. The relation between crack growth resistance and fracture process parameters in elastic-plastic solids. *J. Mech. Phys. Solids*, 40(6):1377–1397, 1992.

[91] V. Tvergaard and J.W. Hutchinson. The influence of plasticity on mixed mode interface toughness. *J. Mech. Phys. Solids*, 41:111911135, 1993.

[92] V. Tvergaard and J.W. Hutchinson. Effect of t-stress on mode i crack growth resistance in a ductile solidg. *Int. J. Solids Struct.*, 31:823833, 1994.

[93] V. Tvergaard and J.W. Hutchinson. Effect of strain-dependent cohesive zone model on predictions of crack growth resistance. *Int. J. Solids Struct.*, 33:3297–3308, 1996.

[94] G.Z. Wang. Effect of martensite transformation on fracture behavior of shape memory alloy NiTi in a notched specimen. *Int. J. Fract.*, 146:93–104, 2007.

[95] G.Z. Wang. A finite element analysis of evolution of stress-strain and martensite transformation in front of a notch in shape memory alloy NiTi. *Mater. Sci. Engng. A*, 460–461:460–461, 2007.

[96] X.M. Wang, Y.F. Wang, A. Baruj, G. Eggeler, and Z.F. Yue. On the formation of martensite in front of cracks in pseudoelastic shape memory alloys. *Mater. Sci. Engng. A*, 394:393–398, 2005.

[97] H.M. Westergaard. Bearing pressures and cracks. *J. Appl. Mech.*, 6:49–53, 1939.

[98] M.I. Williams. On the distribution at the base of a stationary crack. *J. Appl. Mech.*, 24:109–114, 1957.

[99] D. Xie and S. Biggers. Progressive crack growth analysis using interface element based on the virtual crack closure technique. *Finite Elem. Anal. Des.*, 42:977–984, 2006.

[100] F. Xiong and Y. Liu. Effect of stress-induced martensitic transformation on the crack tip stress-intensity factor in Ni-Mn-Ga shape memory alloy. *Acta Mater.*, 55:5621–5629, 2007.

[101] X.P. Xu and A. Needleman. Numerical simulation of fast crack growth in brittle solids. *J. Mech. Phys. Solids*, 42:1397–1434, 1996.

[102] S. Yi and S. Gao. Fracture toughening mechanism of shape memory alloys due to martensite transformation. *Int. J. Solids Struct.*, 37:5315–5327, 2000.

[103] S. Yi, S. Gao, and S. Shen. Fracture toughening mechanism of shape memory alloys under mixed-mode loading due to martensite transformation. *Int. J. Solids Struct.*, 38:4463–4476, 2001.